Boron doping induced thermal conductivity enhancement of water-based 3C-Si(B)C nanofluids

Li, Bin; Jiang, Peng; Zhai, Famin; Chen, Junhong; Bei, Guoping; Hou, Xinmei; Chou, Kuo Chih

Important note
To cite this publication, please use the final published version (if applicable).
Please check the document version above.

1
2
3
4
5
6
...
60

Boron Doping Induced Thermal Conductivity Enhancement of Water-Based 3C-Si(B)C Nanofluids

Bin Li[1,3], Peng Jiang[1], Famin Zhai[1], Junhong Chen[1*], Guoping Bei[2**], Xinmei Hou[3], Kuo-Chih Chou[3]

[1]*School of Materials Science and Engineering, University of Science and Technology Beijing, Beijing, China*

[2]*Department of Materials Science and Engineering, 3ME, Delft University of Technology, Delft, 2628CD, The Netherlands*

[3]*Collaborative Innovation Center of Steel Technology, University of Science and Technology Beijing, Beijing, China*

Abstract

In this paper, the fabrication and thermal conductivity of water-based nanofluids using boron (B) doped SiC as dispersions are reported. Doping B into β-SiC phase leads to the shrinkage of SiC lattice due to the substitution of Si atoms (radius: 0.134 nm) by smaller B atoms (radius: 0.095 nm). The presence of B in SiC phase also promotes crystallization and grain growth of obtained particles. The tailored crystal structure and morphology of B doped SiC nanoparticles are beneficial for the thermal conductivity improvement of the nanofluids by using them as dispersions. Serving B doped SiC nanoparticles as dispersions for nanofluids, a remarkable improvement of the stability was achieved in SiC-B6 nanofluid at pH 11 by means of the Zeta potential measurement. Dispersing B doped SiC nanoparticles in water based fluids, the thermal conductivity of the as prepared nanofluids containing only 0.3 vol. % SiC-B6 nanoparticles is remarkably raised up to 39.3 % at 30 °C compared to the base fluids and is further enhanced with the increased temperature. The main reasons for the improvement of thermal conductivity of SiC-B6 nanofluids are more stable

---
* Author to whom correspondence should be addressed e-mail: cjh2666@126.com (J. H. Chen); Fax: +86 010 6233 2666; Tel: +86 010 6233 2666
** Author to whom correspondence should be addressed e-mail: G.Bei@tudelft.nl (G. P. Bei); Tel: 00 31 15 27 85954

dispersion and intensive charge ions vibration around the surface of nanoparticles as well as the enhanced thermal conductivity of the SiC-B dispersions.

Keywords: Boron doping; SiC nanofluids; Stability; Thermal conductivity.

1. Introduction

Nanofluids, a colloidal mixture with nano-sized solid nanoparticles dispersing in base fluids, have aroused great research interests in recent decades because they can significantly improve the heat transfer characteristics compare to the traditional heat transfer fluids [1-3]. This salient characteristic ensures that the nanofluids have great potential in a variety of thermal exchange systems for different industrial applications such as transportation, electronic cooling, energy storage, mechanical applications and so on. The nanoparticle dispersions used in the nanofluids are typically made of metallic, oxide or non-oxide ceramic nanoparticles while liquids such as water, ethylene glycol, oil, etc. are often adopted as base fluids [4-7]. Ceramic nanoparticle dispersions are more favorable than metallic ones since they can be easily incorporated into the base fluid with better chemical stability over long period of time compared to metallic nanoparticle dispersions[8].

Among those ceramic nanoparticle dispersions, nano-sized silicon carbide (SiC) is one of the most promising dispersions for nanofluids because of its unique properties. SiC is a covalent bond compound that consists of Si and C atoms, with a tetrahedron form in which Si (or C) is the central atom [9]. It has a wide bandgap varying from 2.4 to 3.2 eV depending on the polytype (2.4 eV for 3C-SiC, 3.0 eV for 6H, and 3.2 eV for 4H at 300 K), outstanding electronic features, high thermal conductivity (490 W/m·K) [10-13], excellent oxidation resistance and corrosion durability, great mechanical properties and excellent chemical and physical stability [9, 10, 14, 15]. Extensive research work has been performed to investigate the physical properties of the SiC nanoparticle dispersed nanofluids. Effects of crystal form, particle shape, viscosity, volume concentration, surfactants, base fluid and temperature on the heat transfer performance were studied [16-27]. For example, Timofeeva *et al* [19] demonstrated that the nanofluids with larger particles size and volume concentration provide higher thermal conductivity and lower viscosity increment than those with smaller particles size because of the less solid/liquid interfacial area of larger particles. Li et al investigated the thermos-physical properties of water and Ethylene Glycol (EG) mixture based SiC

nanofluids and found that the thermal conductivity of as prepared nanofluids increased with the volume fraction and the highest thermal conductivity enhancement was found to be 33.84 % for the nanofluid containing 1 vol.% nanosized SiC particles at 20 ^{o}C which indicated that the water/EG based SiC nanofluid might have high potential application for energy system.

The crystal structure, crystallinity and surface property of nanoparticles can be tailored by doping amount of adding ions [28]. However, because of the stronger covalent bond between Si atoms and C atoms, only atoms of some light elements of II-V groups such as B, Be, N, Al having small covalent radius value allowed to be dissolved in the SiC lattice and consequently modify the properties of the SiC particle [28-31]. Thus, in the present study, boron (B), an element from group III in the periodic table of elements, is considered as a dopant for the SiC nanoparticle aiming to improve the surface properties and thermal conductivity of the SiC. Then, those B doped SiC nanoparticles (named SiC-B nanoparticles) will be applied as dispersions for water based nanofluids. The stability and thermal conductivity of nanofluids contained B-doped SiC nanoparticles were determined with different parameters such as B dopant content, the volume concentration of the SiC-B nanoparticles and temperature *etc.*

2. Experimental procedures

2.1 Preparation of nanoparticles

In order to prepare B doped SiC nanoparticles, tetraethyl orthosilicate (TEOS, $(C_2H_5)_4SiO_4$), anhydrous alcohol, tributyl borate ($C_{12}H_{27}BO_3$), hydrogen chloride (HCl) and hydrofluoric acid (HF), purchased from Sinopharm Chemical Reagent Co., Ltd, were adopted as starting materials. In the first step, 25 ml TEOS and 15 ml anhydrous alcohol were mixed by magnetic stirring for 10 minutes followed by adding 15 ml deionized water and 5 ml anhydrous alcohol into the solution and further stirred for 10 min. Afterwards, 5 ml HCl and tributyl borate with different volume amount, i.e. 0, 4, 6 and 8 ml (marked as B0, B4, B6 and B8) were incorporated into the solution by magnetic stirring for another 10 minutes. Finally, 5 g graphite was added in the above solution with 24 hours stirring. The obtained gels were converted into xerogels by drying at 80 °C for 12 hours and pulverized into powders by ball milling. The obtained powders were loaded into corundum crucibles and placed in a vertical tubular furnace and heated to 1500 °C in flowing high purity Ar for 6 hours. The obtained products were further calcined at

700 °C in air for 2 hours to decarburize and then soaked in hydrofluoric (HF) for several hours to remove SiO_2 phase. Finally, the product was cleaned using anhydrous alcohol and deionized water for several times and dried at 70 °C for 12 hours.

2.2 Characterization of nanoparticles

The phases of obtained nanoparticles were identified by X-Ray Diffraction (XRD Bruker D8 Advance) with Cu-Kα radiation. XRD data were refined by using a MAUD software in order to extract the lattice parameter of the B doped 3C-SiC phase [32]. For all the Rietveld refinements in the present work, the two important refinement parameters of the MAUD program, Weighted Reliability factor (*RWP*, %) and Sigma value *(sig.)* were in the 7.37-9.2 % range and 1.43-1.89 range, respectively, indicating reliable Rietveld refinements. Scanning Electron Microscopy (SEM, FEI nova™ nano SEM 450) and High Resolution Transmission Electron Microscopy (HRTEM JEM-1400, JEOL) were applied to characterize the morphologies of the as-synthesized nanoparticles. The crystal structure of the as-prepared SiC-B nanoparticles was determined by mean of Selected Area Electron Diffraction (SAED) equipped on the TEM device, respectively. The elemental composition and bonding configurations of SiC-B nanoparticles were examined by X-ray photoelectron spectroscopy (XPS, Kratos, AXIS ULTRA[DLD]) and Raman spectroscopy (Raman, HORIBA LabRAM HR Evolution) with a wavelength of 325 nm. A Water Contact Angle (WCA) measurement was applied to evaluate the surface property of the as prepared nanoparticles. The measurements were carried out based on the static sessile drop method where water droplets with a volume of 5-10 μL were used. The photographs of water drops were acquired by optical microscopy and three different droplets were applied for each sample.

2.3 Preparation, stability and thermal conductivity of nanofluids

Homogeneous and stable water based nanofluids using nanosized B doped SiC particles (named SiC-B nanofluids) as dispersions were prepared by the two-step method [33]. Depending on the B content in the starting materials, four types of nanofluids (named SiC-B0, SiC-B4, SiC-B6 and SiC-B8 nanofluids, respectively) containing (0 - 0.3) vol.% nanoparticles were prepared and dispersed in deionized water. Ultrasonic homogenization was adopted to achieve a uniform dispersion. Zeta potential and light transmission method were adopted to evaluate the stability of the SiC-B nanofluids. The Zeta potential was performed on a Zeta potential analyzer (Zetasizer, Malvern Nano ZEN 2600), and the effects of the pH values of fluid and concentration were concerned. The light

transmission method was conducted by using a UV spectrophotometer (UV–Vis spectrophotometer, UNIC UV-2800) between 190 and 1100 nm. Thermal Conductivity (TC) of SiC-B nanofluids was measured by using TPS 2500 instrument (Hot Disk model 2500) based on the Transient Plane Source Method (TPS) [34]. The flaky test probe was inserted into the prepared nanofluid with constant temperature, and the TC value of specimen can be obtained by the current response of probe. For each SiC-B nanofluid, 10 TC measurements were performed.

3. Results and Discussion

3.1 Characterization of the B doped SiC nanoparticles

Doping B atom into SiC lattice often leads to a distorted crystal structure of SiC and modifies the surface property and phase composition of the synthesized products. The XRD analysis of the synthesized SiC nanoparticles with variety of B dopant amount (named SiC-B0, SiC-B4, SiC-B6 and SiC-B8) is shown in Fig. 1. It suggested that well crystallized 3C-SiC (β-SiC) phase was formed in all the compositions. A weak diffraction peak of 6H-SiC (α-SiC) at 33.67 ° was also detected in the present XRD patterns which was due to the presence of the stacking faults and the formation of α-SiC phase could be suppressed by doping B element into β-SiC lattice [29, 31, 35]. Such kind of microstructure evolutions were also confirmed by TEM observations. The representative HRTEM micrographs of synthesized nanoparticles (See Fig. 2) clearly reveal that the stacking faults were decreasing gradually as the increasing of B amount. The stacking faults were captured obviously from the B free SiC nanoparticle as shown in Fig. 2(a). However, it can be seen fuzzy stacking faults in the SiC-B6 nanoparticle (Fig. 2(b)) and a neatly arranged lattice structure in the SiC-B8 nanoparticle (Fig. 2(c)) indicating that the presence of B into SiC could eliminate the crystal defects in the grain and stabilize the 3C-SiC (β-SiC) formation in the present study.
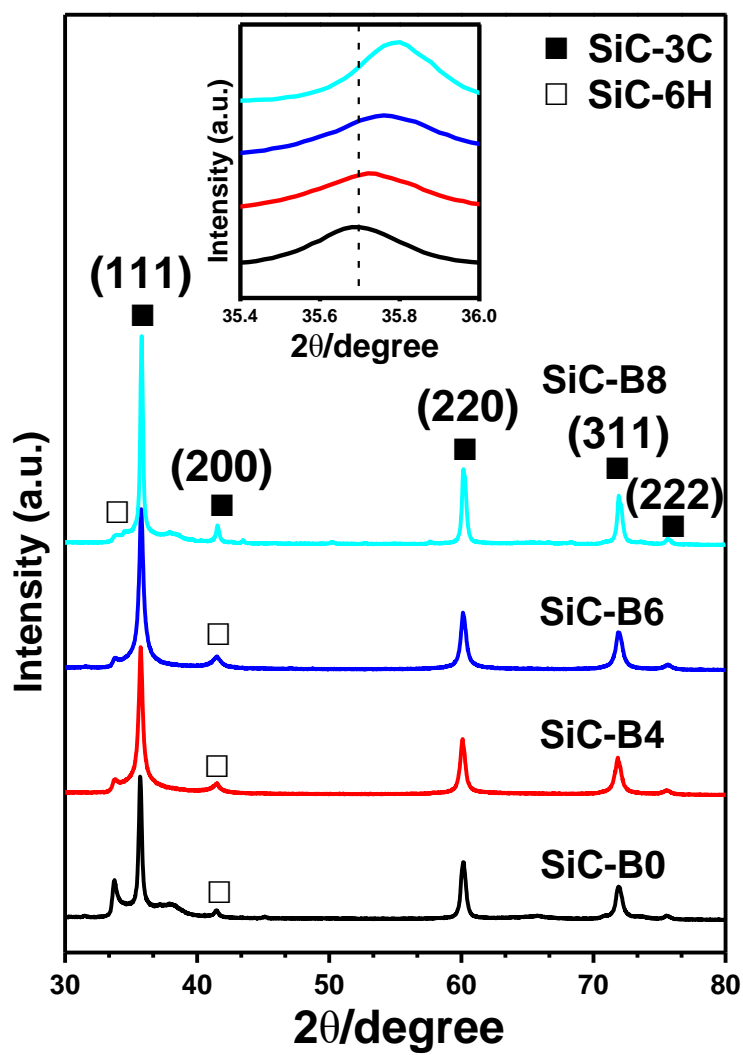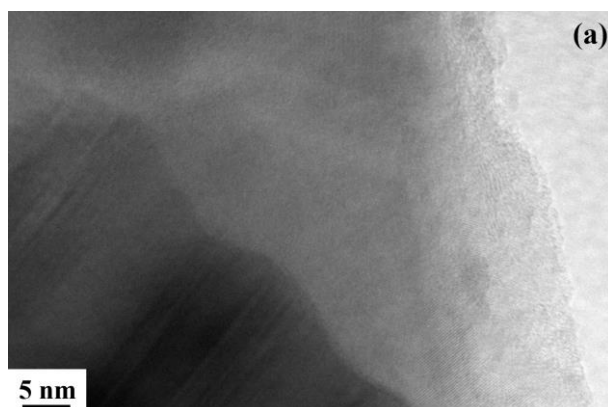
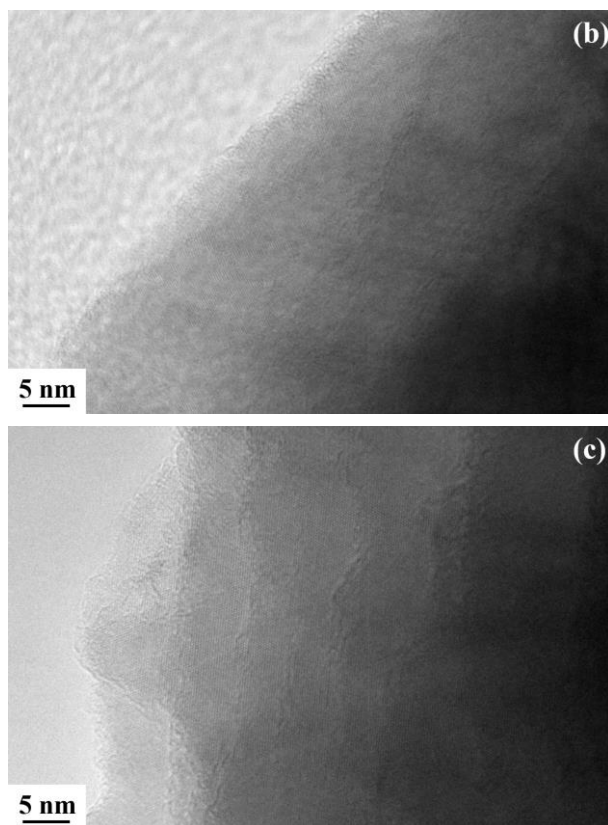Fig. 1: XRD patterns of synthesized B doped SiC nanoparticles.

Fig. 2: HRTEM micrograph of the representing stacking faults in synthesized B doped SiC

nanoparticles, (a) SiC-B0 nanoparticles; (b) SiC-B6 nanoparticles; (c) SiC-B8 nanoparticles.

Another important effect of the B dopant was that the diffraction peaks of 3C-SiC phase were

shifted towards higher diffraction angles with the increasing B dopant content (see the (111) peak

in the inset of Fig. 1). Accommodation of B element into the 3C-SiC crystal structure resulted in

shrinkage of 3C-SiC lattice due to the substitution of Si atoms (radius: 0.134 nm) by smaller B

atoms (radius: 0.095 nm) [28, 29]. Rietveld refinement using the XRD data in a MAUD software

allows to carefully determine the lattice parameter of the 3C-SiC phase.

As an example, Rieveld refined pattern using the XRD data obtained from SiC-B6 (See Fig. 3)

demonstrateda well-fitting between the computed pattern (red line) and the experimental pattern

(blue open circle). Similar Rietveld refinements were performed with other XRD data and the results

are shown Table 1. As expected, the a lattice parameter of SiC-B extracted from the Rietveld

refinement reduced from 4.3550 Å for the SiC without B dopant to 4.3467 Å for SiC-B8

nanoparticle while the inter-planar distance $d_{(111)}$ decreased from 2.5143 Å for the SiC without B

dopant to 2.5096 Å for the SiC-B8 nanoparticle showing a strong modification of the crystal
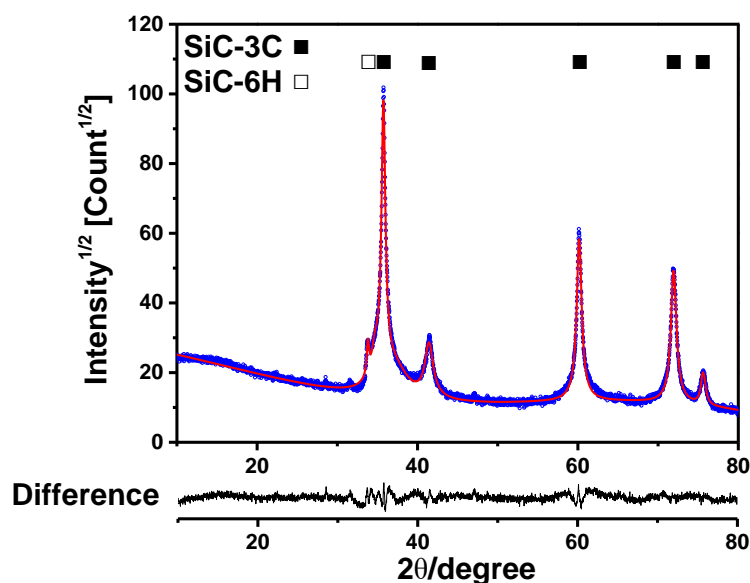
structure of the 3C-SiC phase.

Fig. 3: Rietveld Refinement obtained on the SiC-B6 sample, the red solid line: computed pattern;

blue open circle: experimental data.

Table 1: *a* lattice parameter and inter-planar distance d between (111) planes of 3C-SiC extracted

from Rietveld refinement using a MAUD software.

Starting materials	Rietveld Refinement			
	a lattice parameter (Å)	$d_{(111)}$ (Å)	*Sig*	*RWP(%)*
SiC-B0	4.3550(1)	2.5143	1.78	8.39
SiC-B4	4.3537(5)	2.5136	1.43	7.37
SiC-B6	4.3496(3)	2.5112	1.59	8.1
SiC-B8	4.3467(5)	2.5096	1.89	9.2

The B doped SiC nanoparticles were further characterized by using X-ray photoelectron

spectroscopy (XPS), as shown in Fig. 4. The full XPS spectrum (Fig. 4(a)) shows the existence of

Si, C, B and O for SiC-B4, SiC-B6 and SiC-B8, and Si, C and O exist in SiC-B0. The fine XPS

spectra of Si 2p of SiC-B6 nanoparticles is demonstrated in Fig. 4(b). The peak centered at 100.7

eV corresponds to Si-C bond in SiC, while the peak at 101.8 eV can be assigned to SiO_xC_y [36],

which is the intermediate product during the preparation of SiC nanoparticles. The same analysis

results were obtained from the fine XPS spectra of Si 2p of SiC-B0, SiC-B4 and SiC-B8 (not shown).

Fig. 4(c) gives the fine XPS spectra of B 1s of SiC-B6 nanoparticles. Only one sharp peak appears at 189.8 eV, which can be assigned to the B-C bond in SiC [37, 38]. No peak is detected around 187.4 correspond to the B-Si bond and 193.1 eV correspond to the B-O bond [38], which indicates that B atoms have incorporated into SiC lattice and substituted Si sites. The same analysis results were obtained from the fine XPS spectra of B 1s of SiC-B4 and SiC-B8 (not shown).
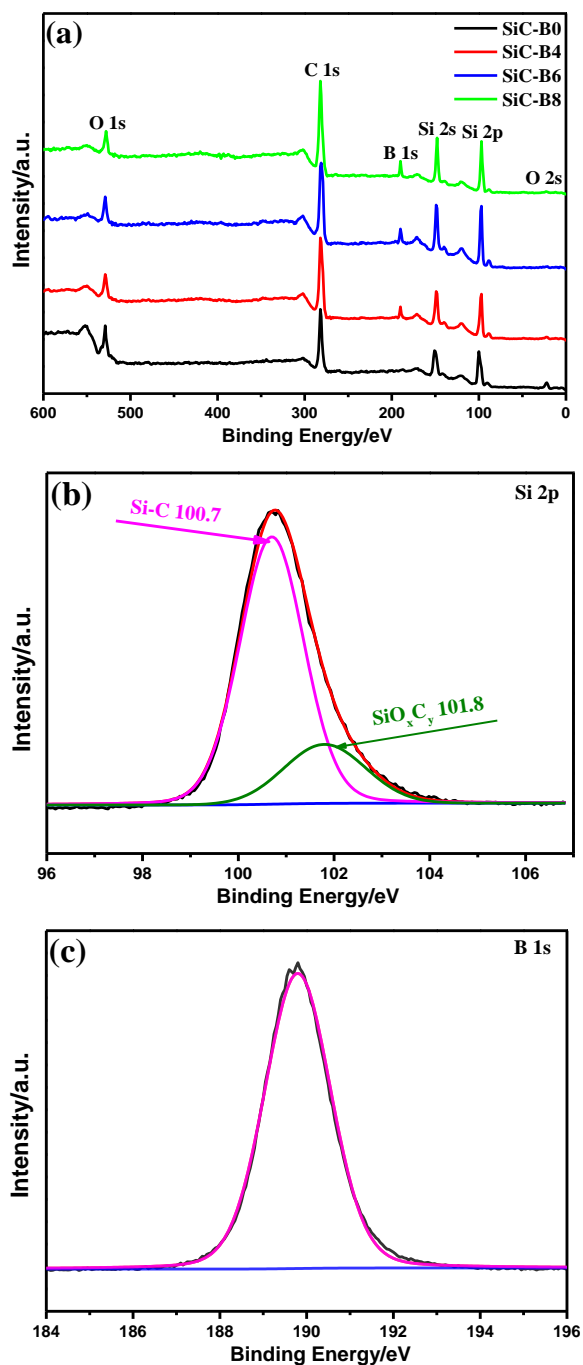
Fig. 4: XPS spectra of synthesized B doped SiC nanoparticles.

Fig. 5 gives the Raman spectra of the synthesized B doped SiC nanoparticles in the $600 \sim 1800$

cm^{-1} region. The Raman spectra shows the presence of sharp peaks at about 790 cm^{-1} and 966 cm^{-1} which correspond to transverse optical (TO) phonon mode and longitudinal optical (LO) phonon mode peaks of β-SiC, respectively [39]. The peak at 1590 cm^{-1} is related to the graphite structure of carbon residual in products, and the peak at 1355 cm^{-1} is similar to the TO peak of diamond, which is indicative of the presence of C–C sp3 bonds in β-SiC. Most probably the bonds are caused by carbon antisites in the SiC structure because of the lowest defect formation energy (1.1 eV) of C_{Si} in β-SiC. The peak intensities at 790 cm^{-1} and 966 cm^{-1} increase with the increasement of B dopant content. It indicates that B doping is beneficial to the crystallization of SiC, which is in agreement with the results of XRD [40]. Additionally, it can be find that the peak at 966 cm^{-1} (LO) shift to higher wavenumber obviously with the increased B dopant content. The LO peak will shift to higher wavenumber as the carrier concentration increases [41], so the LO peak shift of B doped SiC nanoparticles is due to the substitution for B atoms to Si atoms in SiC lattice to form B acceptor doping, resulting in the increase in the carrier concentration of holes. Because of the better crystallization of SiC with B doping, the peak intensity at 1355 cm^{-1} decreases with increasing B content, suggesting the decrease of the amount of C_{Si} defects in SiC crystallite. The peak intensity at 1590 cm^{-1} decreases with the increased B dopant content, which is due to the transformation of the sp2 carbon to the sp3 carbon due to the B doping [42, 43].
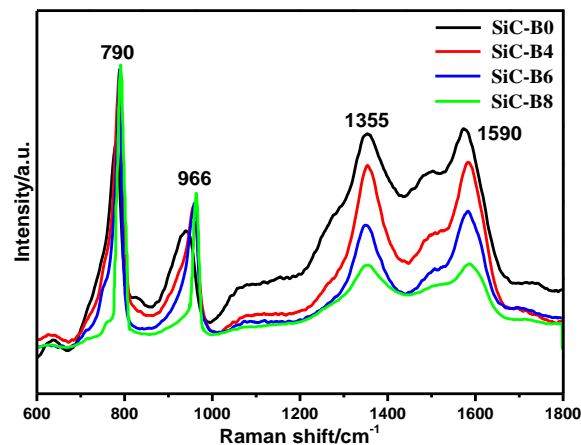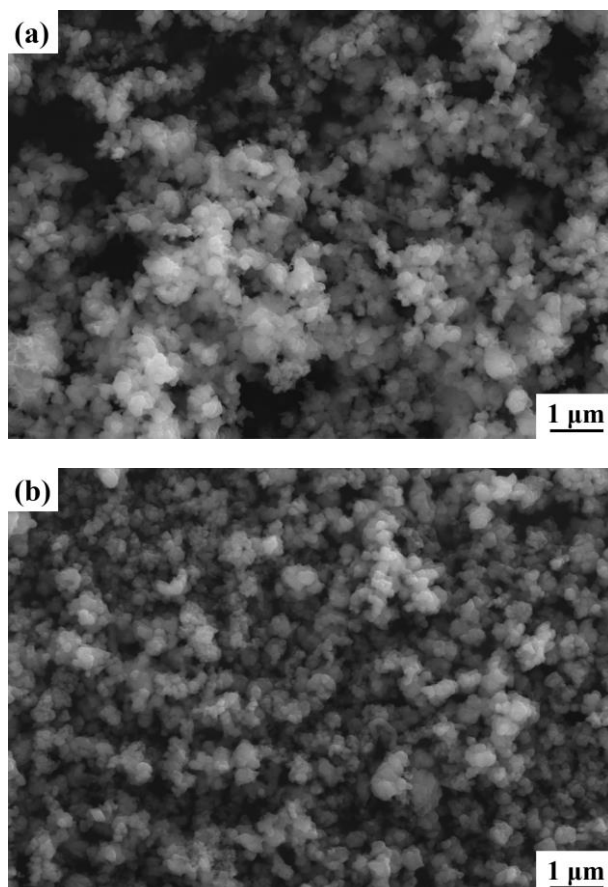

Fig. 5: Raman spectra of synthesized B doped SiC nanoparticles.

The typical microstructures of the obtained SiC-B nanoparticles observed by SEM are revealed in Fig. 6. From Fig. 6(a)-(c), the morphologies of SiC-B nanoparticles did not exhibit varied perceptibly with the increased B dopant content. SiC-B agglomerations consisting of large amount

nanoparticles were observed. Most of the nanoparticles were very smooth with equiaxed round shape. However, great grain growth was observed in the SiC-B8 sample (Fig. 6(d)). Large amount of micron grains with distinctly different shapes, such as plate like shape were observed demonstrating a higher crystallinity and grain growth. Such kind microstructure evolutions were in good agreement with the grain development of B doped SiC during the hot pressing processing and mechanical activation assisted self-propagating high temperature synthesis. It has been reported that the presence of B in SiC matrix could reduce the diffusion activation energy and enhance the mass transportation by several orders of magnitude which promoted the grain growth and crystallization of SiC grains [29, 44, 45]. Fig. 6(e) and Fig. 6(f) give the magnified images of SiC-B8 sample. Form Fig. 6(e), due to the increased tendency of the grains to be crystallized, many larger grains consist of multiple small grains can be seen in SiC-B8. The diameter of larger grains is often more than 1 μm, even close to 2 μm (Fig. 6(f)).

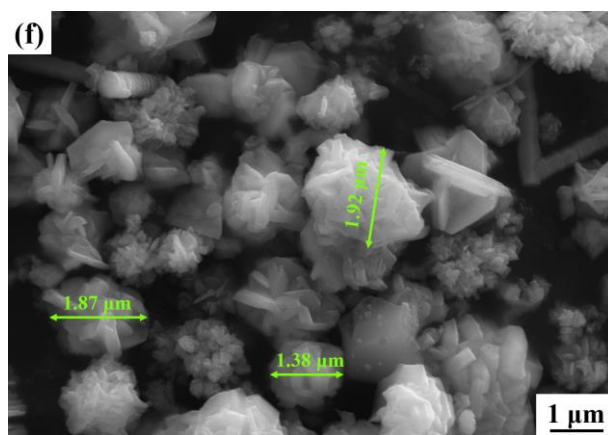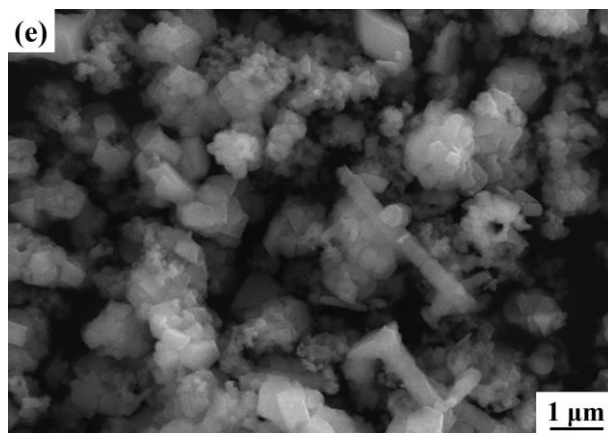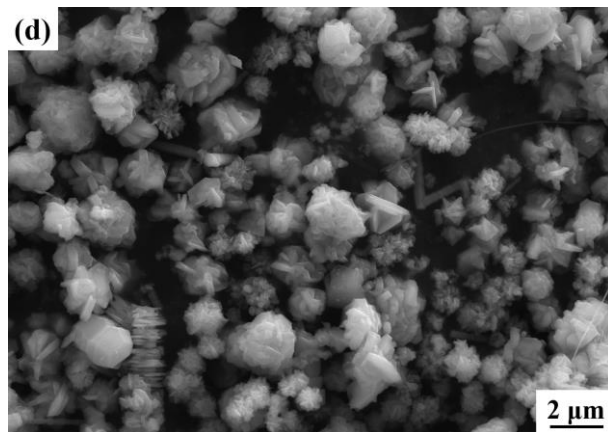Fig. 6: SEM micrographs of synthesized B doped SiC nanoparticles, (a): SiC-B0; (b) SiC-B4; (c)

SiC-B6; (d) SiC-B8; (d) and (e): Magnified images of SiC-B8.

Indeed, the TEM observations and SAED analysis shown in Fig. 7 further confirmed such kind

of microstructural evolutions. In the B free SiC nanoparticle (Fig. 7(a)), the grains are typically

equiaxed shape with an average grain size of 116.33 ± 7.24 nm. However, in the SiC-B4 (not shown)

and SiC-B6 nanoparticle (Fig. 7(c)), elongated grains with an average size of 172.80 ± 33.20 nm

were observed which suggested better crystallization and grain growth. So, over doping B in the

SiC phase would significantly promote grain growth. As shown in the Fig. 7(e), the grains of the

SiC-B8 particles were grown into micron level which was in agreement with the SEM observation.

Furthermore, SAED analysis also shows similar traces. Fig. 7(b) shows a representative diffraction

ring of SiC nanoparticles. However, a clear increase of the diffraction spots was observed in the

diffraction ring patterns of SiC-B6 (Fig. 7(d)) and Si-B8 (Fig. 7(f)) nanoparticles indicating the

improved crystallization of the grains.

Fig. 7: TEM micrographs and SAED patterns of synthesized B doped SiC nanoparticles, (a) and

(b) TEM image and SAED pattern obtained on SiC-B0 nanoparticles; (c) and (d) TEM image and

SAED pattern obtained on SiC-B6 nanoparticles; (e) and (f) TEM image and SAED pattern

obtained on SiC-B8 nanoparticles.
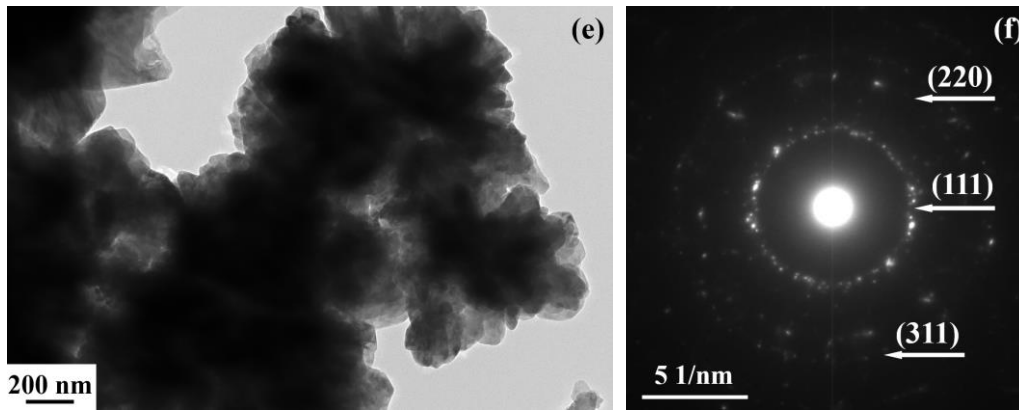
3.2 The surface property of SiC-B nanoparticles

The wettability and hydrophobic property of cubic SiC with different B dopant content are important

factors for water based nanofluid. Water Contact Angle (WCA) are often used to qualify the

properties. The measured WCA of SiC-B nanoparticles with varied B dopant content are shown in

Fig. 8. In the B free SiC nanoparticles, the measured WAC was 115.50 °. However, in the B doped

SiC nanoparticles, the measured WCA of all samples were reduced to almost close to 0 °,

demonstrating that the particles with B dopant possessed good hydrophilicity. According to the

wettability mechanisms, the wettability between the solids and liquid were strongly dependent on

the surface energy of the solid particles. A solid with high surface energy could be easily wetted by

liquid molecular which was due to the improved spreading parameter [46]. In our study, introducing

minor B atoms to replace Si atoms, lattice distortions would take place in the SiC nanoparticles

because a B atom only has three C atoms as neighbors [47]. On the nanoparticles surface and inside,

the atoms near B atoms deviate from their original stable positions, enhancing the surface energy of

SiC nanoparticles. Thus, the improved wettability and hydrophobic property of SiC-B nanoparticles

might be due to the doping the boron into 3C-SiC phase surface which resulted in increase of the

surface energy.

Fig. 8: Measured water contact angles of 3C-SiC-B nanoparticles.

3.3 Stability of SiC-B nanofluids

The stability of nanofluids is a critical factor that must be concerned because of the sedimentation and stratification of nanoparticles which would cause remarkable reduction of the TC of nanofluids and a Zeta potential analysis is commonly applied to evaluate the stability of the nanofluids. In general, a nanofluids with an absolute Zeta potential above 30 mV is considered to have moderate stability and those above 45 mV indicate good stability [22]. The pH value of fluid is a key parameter which affect the Zeta potential and dispersion stability of nanoparticles or colloidal. In order to investigate the stability region and identify the optimized pH values for stable dispersions, Zeta potential analyses of nanofluids containing 0.3 vol % SiC-B nanoparticles were measured in the pH region from 1 to 12 and is shown in Fig. 9(a). The Iso-Electric Points (IEP) for those B-doped SiC nanofluids were around pH 2.4-3.2 and the most stable dispersion was achieved at pH 11. At pH 11, absolute Zeta potential values of 35.5 mV and 23.5 mV were observed in the SiC-B0 nanofluid and SiC-B4 nanofluid, respectively, indicating a moderate stability while an absolute Zeta potential value of 53.5 mV was measured for SiC-B6 nanofluid revealing a superior stability. However, a

significant lower absolute Zeta potential (18.5 mV) was found in the SiC-B8 nanofluid. In the previous study, it has been found the Zeta potential could be strongly affected by the particle size of the dispersions. In the SiC-B8 nanofluid, particle size of the dispersions was over 1 μm, where sedimentation and stratification became pronounced and significantly reduced the stability of the nanofluids.

In addition, the concentration effect on the Zeta potential of the SiC-B nanofluids at pH 11 was shown in the Fig. 9(b). In the 0.1-0.3 vol.% concentration range, the nanofluids with SiC-B6 was found to have highest absolute Zeta potential values compared to the other B doping the SiC nanofluids. The absolute Zeta potential value varied from 47 mV to 52 mV indicating a slight enhancement of the stability with the increased SiC-B6 nanoparticle concentration. However, in the other SiC-B nanofluids, the Zeta potential value did not show improvement within present concentration range and the SiC-B8 nanofluids has the lowest Zeta potential value in the whole range because of the presence of micron size particles.
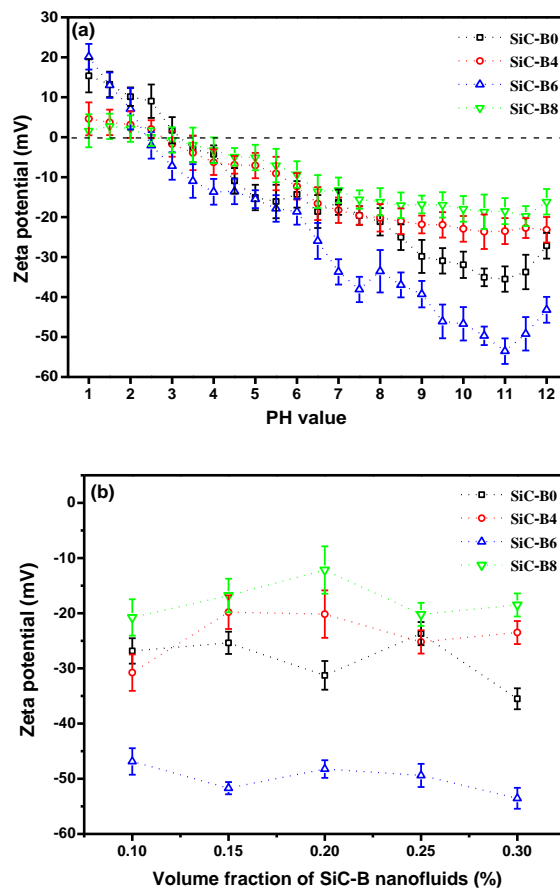

Fig. 9: Zeta potential measurement of B-doped SiC nanofluids, (a) as a function of pH; (b) with different volume fractions of SiC-B nanoparticle dispersions at pH 11.

According to the Beer–Lambert's law [48], the particles concentration is proportional to the absorbance of nanofluids. So, the reduction of particles concentration caused by the instability of nanofluids can be represented by the decrease in absorbance [49]. The relative concentration (C/C_0, the ratio of present concentration to initial concentration) of nanofluids was examined by using UV– vis to describe the stability of SiC-B nanofluids [50]. Fig. 10 illustrates the relative concentrations of SiC-B nanofluids versus time. In the first 3~6 days, the relative concentrations of SiC-B nanofluids decreased continuously, and then they tended to be stable. The SiC-B6 nanofluid exhibits excellent stability performance. In addition to the sedimentation of small amounts of unstable nanoparticles, it maintained a higher relative concentration of 94.72 % after 10 days. However, a very low relative concentration of 23.64 % was obtained from the SiC-B8 nanofluid after 10 days, indicating the poor stability, which is consistent with the analysis of Zeta potential. The sedimentation of many unstable larger particles reduced the relative concentration of SiC-B8 nanofluid. The relative concentrations of SiC-B0 and SiC-B4 nanofluids after 10 days are 69.53 % and 66.89 %, respectively, which are higher than SiC-B8 nanofluid and lower than SiC-B6 nanofluid. The final relative concentrations of SiC-B nanofluids are similar to their results of Zeta potential.

Fig. 10: Relative concentrations f SiC-B nanofluids versus time.

3.4 Thermal conductivity of water-based B-doped SiC nanofluids

The thermal conductivity of water based B-doped SiC nanofluids measured at temperature of 30 °C as a function of volume fractions is shown in Fig. 11(a). The TC values for B-doped SiC nanofluids are higher than that of the base fluids. Meanwhile, the TC of the B-doped SiC nanofluids were improved with the increased concentration of the dispersed nanoparticles in all cases. A remarkable

increase of the TC was observed in the SiC-B6 nanofluid with 0.3 vol.% concentration. Its TC

increases to the highest 0.83 W/m·K with 39.3 % enhancement compare to the base fluids. Such

kind of TC improvement may be due to the better stability and enhanced thermal conductivity of

the SiC-B6 caused by the doping of B in the SiC lattice. However, in the SiC-B8 nanofluids, the TC

was significantly reduced due to the decreased stability which has been indicated by the Zeta

potential measurement. SiC-B8 has the largest crystal size and lowest Zeta potential may lead to

intense aggregation and sedimentation of SiC-B nanoparticle in the base fluid, leading to lower TC

value.

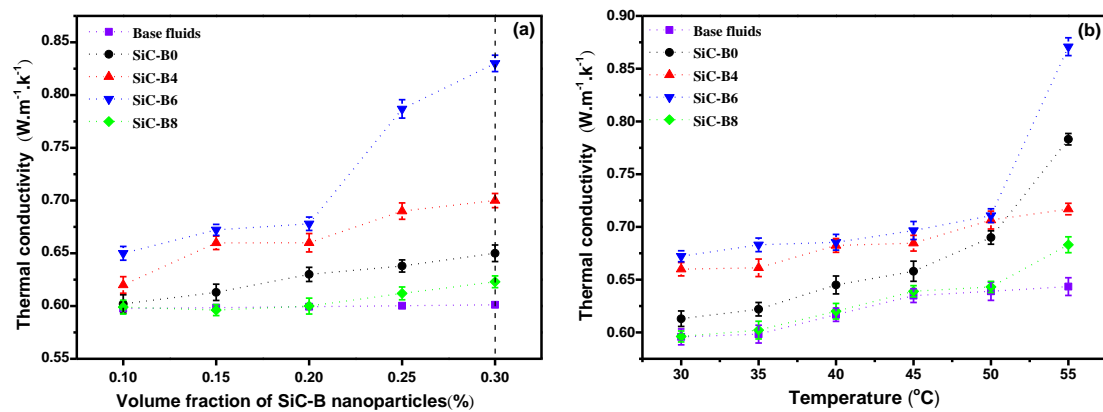Fig. 11: Measured thermal conductivity of water based SiC-B nanofluids as a function of (a)

volume fractions of SiC-B nanoparticle dispersions; (b) temperatures (30-55 °C).

The higher Zeta potential of SiC-B6 nanofluids mean more charge ions are adsorbed on the

surface of nanoparticles in the same base fluid. Therefore,SiC-B6 nanoparticles possess the thickest

stern and gouy layer as shown in Fig. 12. When the nanofluid was working, the charge ions adsorbed

on the surface of nanoparticles transmit heat together with nanoparticles by thermal vibrations,

leading to enhanced thermal conductivity. Furthermore, by doping B in SiC, the TC of the SiC could

be improved. As discussed in the 3.1, the shrinkage of the SiC lattice parameter with the increased

B content suggested that the B element is preferably accommodated in the Si sites because of the

shorter atomic radius of boron. In the unit cell of the SiC, each C atom is connected to four

neighboring Si atoms and each Si atom is connected to four C atoms. Therefore, applying B as

dopant for the SiC, the B atoms will replace the Si atoms and will be connected with neighboring C

atoms. In this case, the difference in the valence between B^{3+} and Si^{4+} will create holes named

"bound holes" [29]. Those "bound holes" could accept electrons and favor thermal motion around the B atoms which can improve the TC of the SiC-B nanoparticles.
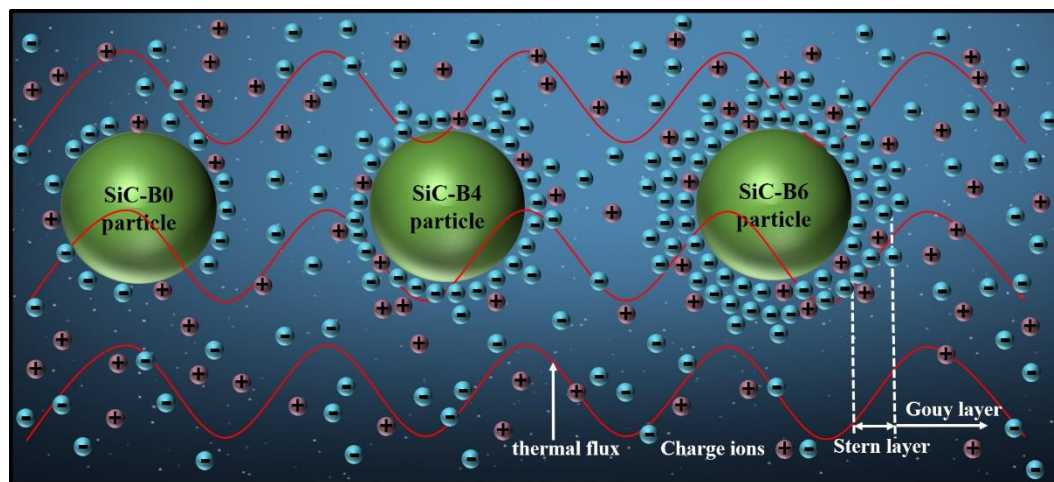

Fig. 12: Schematic diagram of thermal conductivity mechanism SiC-B0, SiC-B4 and SiC-B6 nanofluids

Furthermore, the TC of SiC-B nanofluids with 0.2 vol % nanoparticle concentration measured as a function of temperature is shown in Fig. 11(b). In a temperature range of 30∼55 °C, the TC of SiC-B nanofluids was increased with the increasing temperature in all prepared nanofluids. A significant TC increase was observed in the prepared SiC-B6 nanofluids at 55 °C which was due to acute Brownian motion at higher temperature. Brownian motion of the nanoparticles became drastic with the increased temperature which could provide a much faster heat flow among particles leading to the enhancement of the TC [51]. Moreover, as shown in Table 2, compared with our previous work and aqueous or nonaqueous SiC nanofluids previously reported in the literature [17], SiC-B6 nanofluid with just 0.3 vol % in water can improve the thermal conductivity with the enhancement up to 39.3 % at 30 °C in this work, further verifying the promising application of SiC-B6 nanofluid as thermos-conductive fluids.

Table 2: Comparison of the thermal conductivity of SiC based nanofluids in the literature with this work.

Author	Nanofluid	Concentration	$100(k_{nf}-k_f)/k_f$

Xie et al. [11]	EG/SiC	4.0 vol %	22.90%
Chen et al. [17]	water/SiC	0.3 vol %	13.00%
Yu et al. [18]	EG/SiC	4.0 vol %	67.20%
Timofeeva et al. [19]	water/SiC	4.1 vol %	13.00%
Chen et al. [20]	saline water	0.4 vol %	5.20%
Li et al. [22]	Water/EG/SiC	1.0 vol %	33.84%
Li et al. [25]	EG/SiC	1.0 vol %	16.21%
Lee et al. [27]	water/SiC	3.0 vol %	7.20%
Ghanbarpour et al. [52]	water/SiC	1.0 vol %	29.00%
Singh et al.[53]	water/SiC	7.0 vol %	28.00%
This work	water/SiC	0.3 vol %	39.30%

4. Conclusions

B-doped SiC nanoparticles with varied B content were prepared by carbon thermal reduction reaction at 1500 °C in Ar. The doping of B into SiC phase leads to the shrinkage of crystal lattice of SiC and development of crystallization and grain growth of nanoparticles. From the Zeta potential measurement, a significant improvement of the stability was observed in SiC-B6 nanofluid at pH 11. However, poor stability was found in the over B doped SiC nanofluids (SiC-B8) because of the formation of micron size SiC-B particles which leaded to severe sedimentation and stratification. Furthermore, in the TC measurement of water based SiC-B nanofluids, the TC of the nanofluids containing only 0.3 vol.% SiC-B6 nanoparticles was remarkably improved up to 39.3 % at 30 °C compared to the base fluids and was further raised with the increased temperature. The improvement of TC of SiC-B6 nanofluids were ascribed to the more stable dispersion and more charge ions vibration on the surface of nanoparticles as well as the improvement of thermal conductivity of the SiC-B dispersions.

Acknowledgements

1
2
3
4
5
6
7
8
9
10
11
12
13
14
15
16
17
18
19
20
21
22
23
24
25
26
27
28
29
30
31
32
33
34
35
36
37
38
39
40
41
42
43
44
45
46
47
48
49
50
51
52
53
54
55
56
57
58
59
60

References

[1] Pinto R V and Fiorelli F A S 2016 Review of the mechanisms responsible for heat transfer enhancement using nanofluids *Appl. Therm. Eng.* **108** 720-39

[2] Haddad Z, Abid C, Oztop H F and Mataoui A 2014 A review on how the researchers prepare their nanofluids *Int J Therm Sci* **76** 168-89

[3] Babita, Sharma S K and Gupta S M 2016 Preparation and evaluation of stable nanofluids for heat transfer application: A review *Exp. Therm Fluid Sci.* **79** 202-12

[4] Taylor R, Coulombe S, Otanicar T, Phelan P, Gunawan A, Lv W, Rosengarten G, Prasher R and Tyagi H 2013 Small particles, big impacts: A review of the diverse applications of nanofluids *J. Appl. Phys.* **113**

[5] Lee D, Park J-J, Lee M-K and Lee G-J 2017 Aging-resistant nanofluids containing covalent functionalized boron nitride nanosheets *Nanotechnology* **28** 405704

[6] Ismail A M, Emara M M, El din Kassem T S and Moussa M A 2017 How assembly matters to catalysis and thermal conductivity mediated by CuO nanoparticles *Nanotechnology* **28** 075705

[7] Karthikeyan A, Coulombe S and Kietzig A 2017 Wetting behavior of multi-walled carbon nanotube nanofluids *Nanotechnology* **28** 105706

[8] Yoo D H, Hong K S and Yang H S 2007 Study of thermal conductivity of nanofluids for the application of heat transfer fluids *Thermochim. Acta* **455** 66-9

[9] Izhevskyi V A, Genova L A, Bressiani J C and Bressiani A H A 2000 Review article: silicon carbide. Structure, properties and processing *Cerâmica* **46** 4-13

[10] Park C H, Cheong B H, Lee K H and Chang K J 1994 Structural and electronic properties of cubic, 2H, 4H, and 6H SiC *Phys Rev B Condens Matter* **49** 4485-93

[11] Xie H, Wang J, Xi T and Liu Y 2002 Thermal conductivity of suspensions containing nanosized SiC particles *Int. J. Thermophys.* **23** 571-80

[12] Roy S, Jacob C and Basu S 2004 Current transport properties of Pd/3C–SiC Schottky junctions with planar and vertical structures *Solid State Sciences* **6** 377-82

[13] Su J F, Niu Q, Tang C J, Zhang Y S and Fu Z X 2012 Growth of void-free 3C-SiC films by modified two-step carbonization methods *Solid State Sciences* **14** 545-9

[14] Eddy C R and Gaskill D K 2009 Silicon Carbide as a Platform for Power Electronics *Science* **324** 1398-400

[15] Wu R B, Zhou K, Yue C Y, Wei J and Pan Y 2015 Recent progress in synthesis, properties and potential applications of SiC nanomaterials *Prog. Mater Sci.* **72** 1-60

[16] Nikkam N, Haghighi E B, Saleemi M, Behi M, Khodabandeh R, Muhammed M, Palm B and Toprak M S 2014 Experimental study on preparation and base liquid effect on thermo-physical and heat transport characteristics of α-SiC nanofluids ☆ *International Communications in Heat & Mass Transfer* **55** 38-44

[17] Chen J H, Zhai F M, Liu M, Hou X M and Chou K C 2016 SiC nanowires with tunable hydrophobicity/hydrophilicity and their application as nanofluids *Langmuir* **32** 5909-16

[18] Yu W, Wang M Z, Xie H Q, Hu Y H and Chen L F 2016 Silicon carbide nanowires suspensions with high thermal transport properties *Appl. Therm. Eng.* **94** 350-4

[19] Timofeeva E V, Smith D S, Yu W, France D M, Singh D and Routbort J L 2010 Particle size and interfacial effects on thermo-physical and heat transfer characteristics of water-based α-SiC nanofluids *Nanotechnology* **21** 215703

[20] Chen W J, Zou C J, Li X K and Li L 2017 Experimental investigation of SiC nanofluids for solar distillation system: Stability, optical properties and thermal conductivity with saline water based fluid *Int. J. Heat Mass Transfer* **107** 264-70

[21] Li X K, Zou C J, Zhou L and Qi A H 2016 Experimental study on the thermo-physical properties of diathermic oil based SiC nanofluids for high temperature applications *Int. J. Heat Mass Transfer* **97** 631-7

[22] Li X K and Zou C J 2016 Thermo-physical properties of water and ethylene glycol mixture based SiC nanofluids: An experimental investigation *Int. J. Heat Mass Transfer* **101** 412-7

[23] Li X K, Zou C J and Qi A H 2016 Experimental study on the thermo-physical properties of car engine coolant (water/ethylene glycol mixture type) based SiC nanofluids *Int. Commun. Heat Mass* **77** 159-64

[24] Li X K, Zou C J, Wang T Y and Lei X Y 2015 Rheological behavior of ethylene glycol-based SiC nanofluids *Int. J. Heat Mass Transfer* **84** 925-30

[25] Li X K, Zou C J, Lei X Y and Li W L 2015 Stability and enhanced thermal conductivity of ethylene glycol-based SiC nanofluids *Int. J. Heat Mass Transfer* **89** 613-9

[26] Timofeeva E V, Yu W H, France D M, Singh D and Routbort J L 2011 Base fluid and temperature effects on the heat transfer characteristics of SiC in ethylene glycol/H_2O and H_2O nanofluids *J. Appl. Phys.* **109**

[27] Lee S W, Park S D, Kang S, Bang I C and Kim J H 2011 Investigation of viscosity and thermal conductivity of SiC nanofluids for heat transfer applications *Int. J. Heat Mass Transfer* **54** 433-8

[28] Yang T, Zhang L, Hou X, Chen J and Chou K C 2016 Bare and boron-doped cubic silicon carbide nanowires for electrochemical detection of nitrite sensitively *Sci Rep* **6** 24872

[29] Agathopoulos S 2012 Influence of synthesis process on the dielectric properties of B-doped SiC powders *Ceram. Int.* **38** 3309-15

[30] Kim K J, Lim K Y, Kim Y W and Kim H C 2013 Temperature Dependence of Electrical Resistivity (4–300K) in Aluminum- and Boron-Doped SiC Ceramics *J. Am. Ceram. Soc.* **96** 2525–30

[31] Gadzira M, Gnesin G, Mykhaylyk O and Andreyev O 1998 Synthesis and structural peculiarities of nonstoichiometric β-SiC *Diamond & Related Materials* **7** 1466-70

[32] Lutterotti L, Matthies S and Wenk H 1999 MAUD: a friendly Java program for material analysis using diffraction *CPD NEWSLETTER* **21** 14-5

[33] Mahbubul I M, Saidur R and Amalina M A 2012 Latest developments on the viscosity of nanofluids *Int. J. Heat Mass Transfer* **55** 874-85

[34] Log T and Gustafsson S E 1995 Transient plane source (TPS) technique for measuring thermal transport properties of building materials *Fire & Materials* **19** 43–9

[35] Su X L, Zhou W C, Xu J, Li Z M, Luo F and Zhu D M 2010 Improvement of permittivity of SiC with Al doping by combustion synthesis using Al_2O_3 *J. Alloys Compd.* **492** L16-L9

[36] Shimoda K, Park J S, Hinoki T and Kohyama A 2007 Influence of surface structure of SiC nano-

sized powder analyzed by X-ray photoelectron spectroscopy on basic powder characteristics *Appl. Surf. Sci.* **253** 9450-6

[37] Dong L L, Wang Y Y, Tong X L, Jin G Q and Guo X Y 2014 Synthesis and characterization of boron-doped SiC for visible light driven hydrogen production *Acta Physico-Chimica Sinica* **30** 135-40

[38] Oswald S and Wirth H 1999 Core-level shifts at B- and Al-doped 6H-SiC studied by XPS *Surf. Interface Anal.* **27** 136-41

[39] Li Z M, Zhou W C, Su X L, Luo F, Huang Y X and Wang C 2011 Effect of boron doping on microwave dielectric properties of SiC powder synthesized by combustion synthesis *J. Alloys Compd.* **509** 973-6

[40] Su X L, Zhou W C, Li Z M, Luo F, Du H L and Zhu D M 2009 Preparation and dielectric properties of B-doped SiC powders by combustion synthesis *Mater. Res. Bull.* **44** 880-3

[41] Li Z, Zhou W, Lei T, Luo F, Huang Y and Cao Q 2009 Microwave dielectric properties of SiC(B) solid solution powder prepared by sol–gel *J. Alloys Compd.* **475** 506-9

[42] Beeman D, Silverman J, Lynds R and Anderson M R 1984 Modeling studies of amorphous carbon *Phys. Rev. B* **30** 870-5

[43] Richter A, Scheibe H J, Pompe W, Brzezinka K W and Mühling I 1986 About the structure and bonding of laser generated carbon films by raman and electron energy loss spectroscopy *J. Non-Cryst. Solids* **88** 131-44

[44] Maître A, Put A V, Laval J P, Valette S and Trolliard G 2008 Role of boron on the Spark Plasma Sintering of an α-SiC powder *J. Eur. Ceram. Soc.* **28** 1881-90

[45] Datta M S, Bandyopadhyay A K and Chaudhuri B 2002 Sintering of nano crystalline α silicon carbide by doping with boron carbide *Bull. Mater. Sci.* **25** 181-9

[46] Gennes P G D 1985 Wetting: Static and Dynamics *Review of Modern Physics* **57** 827-63

[47] Rurali R, Hernandez E, Godignon P, Rebollo J and Ordejon P 2004 First-principles studies of the diffusion of B impurities and vacancies in SiC *Phys. Rev. B* **69**

[48] Aravind S S J, Baskar P, Baby T T, Sabareesh R K, Das S and Ramaprabhu S 2011 Investigation of Structural Stability, Dispersion, Viscosity, and Conductive Heat Transfer Properties of Functionalized Carbon Nanotube Based Nanofluids *The Journal of Physical Chemistry C* **115** 16737-44

[49] Mehrali M, Sadeghinezhad E, Rosen M A, Akhiani A R, Tahan Latibari S, Mehrali M and Metselaar H S C 2016 Experimental investigation of thermophysical properties, entropy generation and convective heat transfer for a nitrogen-doped graphene nanofluid in a laminar flow regime *Adv. Powder Technol.* **27** 717-27

[50] Sadeghinezhad E, Mehrali M, Akhiani A R, Tahan Latibari S, Dolatshahi-Pirouz A, Metselaar H S C and Mehrali M 2017 Experimental study on heat transfer augmentation of graphene based ferrofluids in presence of magnetic field *Appl. Therm. Eng.* **114** 415-27

[51] Vajjha R S and Das D K 2012 A review and analysis on influence of temperature and concentration of nanofluids on thermophysical properties, heat transfer and pumping power *Int. J. Heat Mass Transfer* **55** 4063-78

[52] Ghanbarpour M, Nikkam N, Khodabandeh R and Toprak M S 2015 Improvement of heat transfer characteristics of cylindrical heat pipe by using SiC nanofluids *Appl. Therm. Eng.* **90** 127-35

[53] Singh D, Timofeeva E, Yu W, Routbort J, France D, Smith D and Lopez-Cepero J M 2009 An

investigation of silicon carbide-water nanofluid for heat transfer applications *J. Appl. Phys.* **105**

Boron Doping Induced Thermal Conductivity Enhancement of Water-Based 3C-Si(B)C Nanofluids

Bin Li[1,3], Peng Jiang[1], Famin Zhai[1], Junhong Chen[1*], Guoping Bei[2**], Xinmei Hou[3], Kuo-Chih Chou[3]

[1]*School of Materials Science and Engineering, University of Science and Technology Beijing, Beijing, China*

[2]*Department of Materials Science and Engineering, 3ME, Delft University of Technology, Delft, 2628CD, The Netherlands*

[3]*Collaborative Innovation Center of Steel Technology, University of Science and Technology Beijing, Beijing, China*

Abstract

In this paper, the fabrication and thermal conductivity of water-based nanofluids using boron (B) doped SiC as dispersions are reported. Doping B into β-SiC phase leads to the shrinkage of SiC lattice due to the substitution of Si atoms (radius: 0.134 nm) by smaller B atoms (radius: 0.095 nm). The presence of B in SiC phase also promotes crystallization and grain growth of obtained particles. The tailored crystal structure and morphology of B doped SiC nanoparticles are beneficial for the thermal conductivity improvement of the nanofluids by using them as dispersions. Serving B doped SiC nanoparticles as dispersions for nanofluids, a remarkable improvement of the stability was achieved in SiC-B6 nanofluid at pH 11 by means of the Zeta potential measurement. Dispersing B doped SiC nanoparticles in water based fluids, the thermal conductivity of the as prepared nanofluids containing only 0.3 vol. % SiC-B6 nanoparticles is remarkably raised up to 39.3 % at 30 °C compared to the base fluids and is further enhanced with the increased temperature. The main reasons for the improvement of thermal conductivity of SiC-B6 nanofluids are more stable

---

* Author to whom correspondence should be addressed e-mail: cjh2666@126.com (J. H. Chen); Fax: +86 010 6233 2666; Tel: +86 010 6233 2666

** Author to whom correspondence should be addressed e-mail: G.Bei@tudelft.nl (G. P. Bei); Tel: 00 31 15 27 85954

dispersion and intensive charge ions vibration around the surface of nanoparticles as well as the enhanced thermal conductivity of the SiC-B dispersions.

Keywords: Boron doping; SiC nanofluids; Stability; Thermal conductivity.

1. Introduction

Nanofluids, a colloidal mixture with nano-sized solid nanoparticles dispersing in base fluids, have aroused great research interests in recent decades because they can significantly improve the heat transfer characteristics compare to the traditional heat transfer fluids [1-3]. This salient characteristic ensures that the nanofluids have great potential in a variety of thermal exchange systems for different industrial applications such as transportation, electronic cooling, energy storage, mechanical applications and so on. The nanoparticle dispersions used in the nanofluids are typically made of metallic, oxide or non-oxide ceramic nanoparticles while liquids such as water, ethylene glycol, oil, etc. are often adopted as base fluids [4-7]. Ceramic nanoparticle dispersions are more favorable than metallic ones since they can be easily incorporated into the base fluid with better chemical stability over long period of time compared to metallic nanoparticle dispersions[8].

Among those ceramic nanoparticle dispersions, nano-sized silicon carbide (SiC) is one of the most promising dispersions for nanofluids because of its unique properties. SiC is a covalent bond compound that consists of Si and C atoms, with a tetrahedron form in which Si (or C) is the central atom [9]. It has a wide bandgap varying from 2.4 to 3.2 eV depending on the polytype (2.4 eV for 3C-SiC, 3.0 eV for 6H, and 3.2 eV for 4H at 300 K), outstanding electronic features, high thermal conductivity (490 W/m·K) [10-13], excellent oxidation resistance and corrosion durability, great mechanical properties and excellent chemical and physical stability [9, 10, 14, 15]. Extensive research work has been performed to investigate the physical properties of the SiC nanoparticle dispersed nanofluids. Effects of crystal form, particle shape, viscosity, volume concentration, surfactants, base fluid and temperature on the heat transfer performance were studied [16-27]. For example, Timofeeva *et al* [19] demonstrated that the nanofluids with larger particles size and volume concentration provide higher thermal conductivity and lower viscosity increment than those with smaller particles size because of the less solid/liquid interfacial area of larger particles. Li et al investigated the thermos-physical properties of water and Ethylene Glycol (EG) mixture based SiC

nanofluids and found that the thermal conductivity of as prepared nanofluids increased with the volume fraction and the highest thermal conductivity enhancement was found to be 33.84 % for the nanofluid containing 1 vol.% nanosized SiC particles at 20 °C which indicated that the water/EG based SiC nanofluid might have high potential application for energy system.

The crystal structure, crystallinity and surface property of nanoparticles can be tailored by doping amount of adding ions [28]. However, because of the stronger covalent bond between Si atoms and C atoms, only atoms of some light elements of II-V groups such as B, Be, N, Al having small covalent radius value allowed to be dissolved in the SiC lattice and consequently modify the properties of the SiC particle [28-31]. Thus, in the present study, boron (B), an element from group III in the periodic table of elements, is considered as a dopant for the SiC nanoparticle aiming to improve the surface properties and thermal conductivity of the SiC. Then, those B doped SiC nanoparticles (named SiC-B nanoparticles) will be applied as dispersions for water based nanofluids. The stability and thermal conductivity of nanofluids contained B-doped SiC nanoparticles were determined with different parameters such as B dopant content, the volume concentration of the SiC-B nanoparticles and temperature *etc.*

2. Experimental procedures

2.1 Preparation of nanoparticles

In order to prepare B doped SiC nanoparticles, tetraethyl orthosilicate (TEOS, $(C_2H_5)_4SiO_4$), anhydrous alcohol, tributyl borate ($C_{12}H_{27}BO_3$), hydrogen chloride (HCl) and hydrofluoric acid (HF), purchased from Sinopharm Chemical Reagent Co., Ltd, were adopted as starting materials. In the first step, 25 ml TEOS and 15 ml anhydrous alcohol were mixed by magnetic stirring for 10 minutes followed by adding 15 ml deionized water and 5 ml anhydrous alcohol into the solution and further stirred for 10 min. Afterwards, 5 ml HCl and tributyl borate with different volume amount, i.e. 0, 4, 6 and 8 ml (marked as B0, B4, B6 and B8) were incorporated into the solution by magnetic stirring for another 10 minutes. Finally, 5 g graphite was added in the above solution with 24 hours stirring. The obtained gels were converted into xerogels by drying at 80 °C for 12 hours and pulverized into powders by ball milling. The obtained powders were loaded into corundum crucibles and placed in a vertical tubular furnace and heated to 1500 °C in flowing high purity Ar for 6 hours. The obtained products were further calcined at

700 °C in air for 2 hours to decarburize and then soaked in hydrofluoric (HF) for several hours to remove SiO_2 phase. Finally, the product was cleaned using anhydrous alcohol and deionized water for several times and dried at 70 °C for 12 hours.

2.2 Characterization of nanoparticles

The phases of obtained nanoparticles were identified by X-Ray Diffraction (XRD Bruker D8 Advance) with Cu-Kα radiation. XRD data were refined by using a MAUD software in order to extract the lattice parameter of the B doped 3C-SiC phase [32]. For all the Rietveld refinements in the present work, the two important refinement parameters of the MAUD program, Weighted Reliability factor (*RWP*, %) and Sigma value *(sig.)* were in the 7.37-9.2 % range and 1.43-1.89 range, respectively, indicating reliable Rietveld refinements. Scanning Electron Microscopy (SEM, FEI nova™ nano SEM 450) and High Resolution Transmission Electron Microscopy (HRTEM JEM-1400, JEOL) were applied to characterize the morphologies of the as-synthesized nanoparticles. The crystal structure of the as-prepared SiC-B nanoparticles was determined by mean of Selected Area Electron Diffraction (SAED) equipped on the TEM device, respectively. The elemental composition and bonding configurations of SiC-B nanoparticles were examined by X-ray photoelectron spectroscopy (XPS, Kratos, AXIS ULTRA[DLD]) and Raman spectroscopy (Raman, HORIBA LabRAM HR Evolution) with a wavelength of 325 nm. A Water Contact Angle (WCA) measurement was applied to evaluate the surface property of the as prepared nanoparticles. The measurements were carried out based on the static sessile drop method where water droplets with a volume of 5-10 μL were used. The photographs of water drops were acquired by optical microscopy and three different droplets were applied for each sample.

2.3 Preparation, stability and thermal conductivity of nanofluids

Homogeneous and stable water based nanofluids using nanosized B doped SiC particles (named SiC-B nanofluids) as dispersions were prepared by the two-step method [33]. Depending on the B content in the starting materials, four types of nanofluids (named SiC-B0, SiC-B4, SiC-B6 and SiC-B8 nanofluids, respectively) containing (0 - 0.3) vol.% nanoparticles were prepared and dispersed in deionized water. Ultrasonic homogenization was adopted to achieve a uniform dispersion. Zeta potential and light transmission method were adopted to evaluate the stability of the SiC-B nanofluids. The Zeta potential was performed on a Zeta potential analyzer (Zetasizer, Malvern Nano ZEN 2600), and the effects of the pH values of fluid and concentration were concerned. The light

transmission method was conducted by using a UV spectrophotometer (UV–Vis spectrophotometer, UNIC UV-2800) between 190 and 1100 nm. Thermal Conductivity (TC) of SiC-B nanofluids was measured by using TPS 2500 instrument (Hot Disk model 2500) based on the Transient Plane Source Method (TPS) [34]. The flaky test probe was inserted into the prepared nanofluid with constant temperature, and the TC value of specimen can be obtained by the current response of probe. For each SiC-B nanofluid, 10 TC measurements were performed.

3. Results and Discussion

3.1 Characterization of the B doped SiC nanoparticles

Doping B atom into SiC lattice often leads to a distorted crystal structure of SiC and modifies the surface property and phase composition of the synthesized products. The XRD analysis of the synthesized SiC nanoparticles with variety of B dopant amount (named SiC-B0, SiC-B4, SiC-B6 and SiC-B8) is shown in Fig. 1. It suggested that well crystallized 3C-SiC (β-SiC) phase was formed in all the compositions. A weak diffraction peak of 6H-SiC (α-SiC) at 33.67 ° was also detected in the present XRD patterns which was due to the presence of the stacking faults and the formation of α-SiC phase could be suppressed by doping B element into β-SiC lattice [29, 31, 35]. Such kind of microstructure evolutions were also confirmed by TEM observations. The representative HRTEM micrographs of synthesized nanoparticles (See Fig. 2) clearly reveal that the stacking faults were decreasing gradually as the increasing of B amount. The stacking faults were captured obviously from the B free SiC nanoparticle as shown in Fig. 2(a). However, it can be seen fuzzy stacking faults in the SiC-B6 nanoparticle (Fig. 2(b)) and a neatly arranged lattice structure in the SiC-B8 nanoparticle (Fig. 2(c)) indicating that the presence of B into SiC could eliminate the crystal defects in the grain and stabilize the 3C-SiC (β-SiC) formation in the present study.
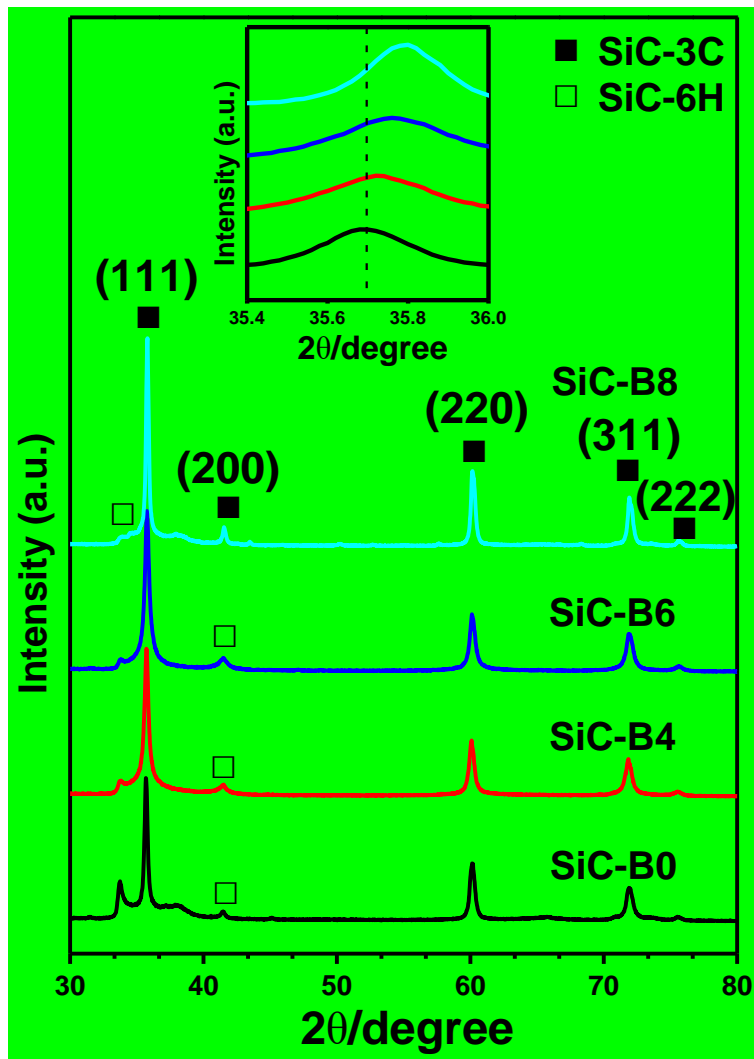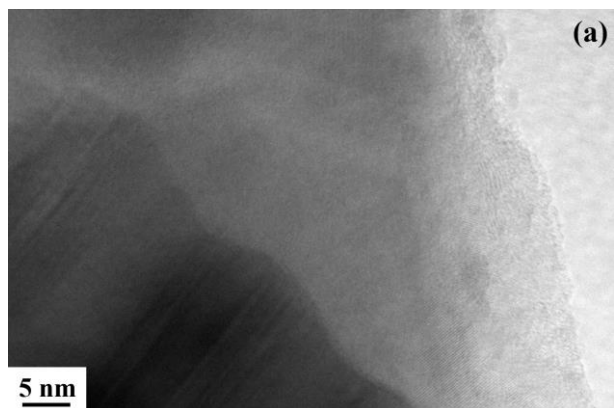
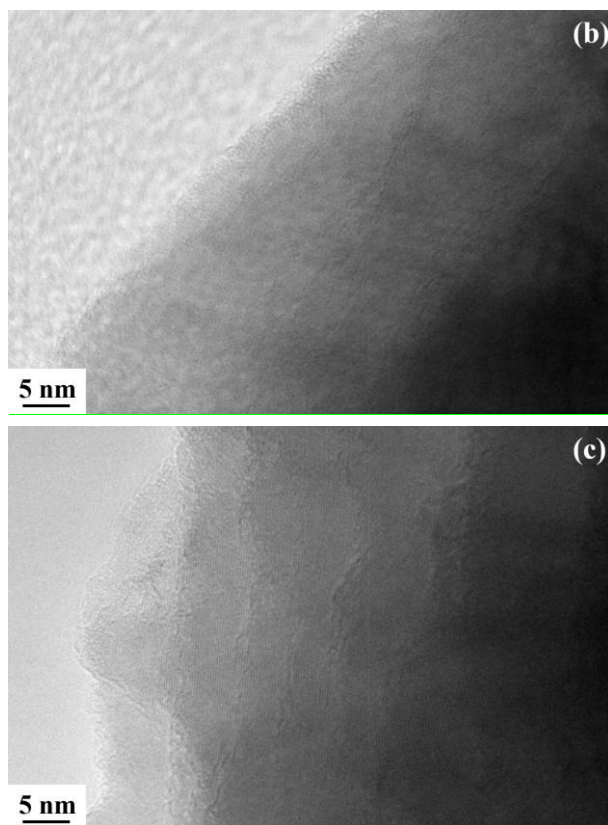Fig. 1: XRD patterns of synthesized B doped SiC nanoparticles.

Fig. 2: HRTEM micrograph of the representing stacking faults in synthesized B doped SiC nanoparticles, (a) SiC-B0 nanoparticles; (b) SiC-B6 nanoparticles; (c) SiC-B8 nanoparticles.

Another important effect of the B dopant was that the diffraction peaks of 3C-SiC phase were shifted towards higher diffraction angles with the increasing B dopant content (see the (111) peak in the inset of Fig. 1). Accommodation of B element into the 3C-SiC crystal structure resulted in shrinkage of 3C-SiC lattice due to the substitution of Si atoms (radius: 0.134 nm) by smaller B atoms (radius: 0.095 nm) [28, 29]. Rietveld refinement using the XRD data in a MAUD software allows to carefully determine the lattice parameter of the 3C-SiC phase.

As an example, Rieveld refined pattern using the XRD data obtained from SiC-B6 (See Fig. 3) demonstrateda well-fitting between the computed pattern (red line) and the experimental pattern (blue open circle). Similar Rietveld refinements were performed with other XRD data and the results are shown Table 1. As expected, the a lattice parameter of SiC-B extracted from the Rietveld refinement reduced from 4.3550 Å for the SiC without B dopant to 4.3467 Å for SiC-B8 nanoparticle while the inter-planar distance $d_{(111)}$ decreased from 2.5143 Å for the SiC without B dopant to 2.5096 Å for the SiC-B8 nanoparticle showing a strong modification of the crystal
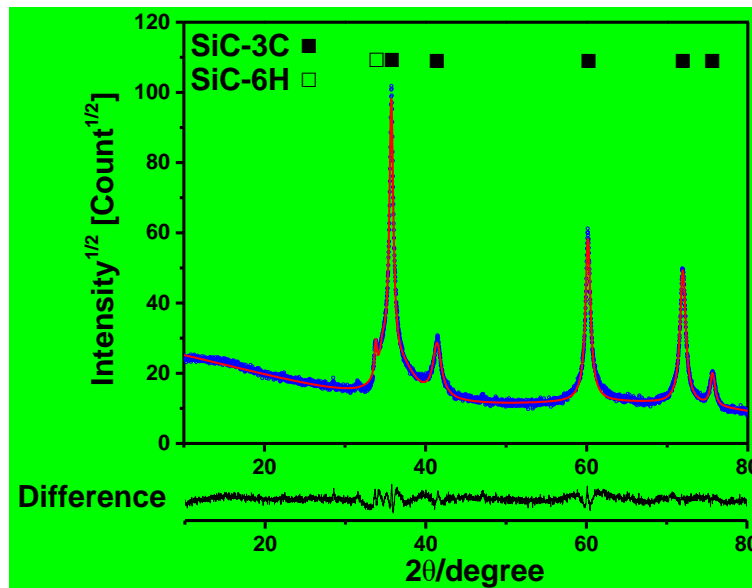
structure of the 3C-SiC phase.

Fig. 3: Rietveld Refinement obtained on the SiC-B6 sample, the red solid line: computed pattern;

blue open circle: experimental data.

Table 1: *a* lattice parameter and inter-planar distance d between (111) planes of 3C-SiC extracted

from Rietveld refinement using a MAUD software.

Starting materials	Rietveld Refinement			
	a lattice parameter (Å)	d*(111)* (Å)	*Sig*	*RWP(%)*
SiC-B0	4.3550(1)	2.5143	1.78	8.39
SiC-B4	4.3537(5)	2.5136	1.43	7.37
SiC-B6	4.3496(3)	2.5112	1.59	8.1
SiC-B8	4.3467(5)	2.5096	1.89	9.2

The B doped SiC nanoparticles were further characterized by using X-ray photoelectron spectroscopy (XPS), as shown in Fig. 4. The full XPS spectrum (Fig. 4(a)) shows the existence of Si, C, B and O for SiC-B4, SiC-B6 and SiC-B8, and Si, C and O exist in SiC-B0. The fine XPS spectra of Si 2p of SiC-B6 nanoparticles is demonstrated in Fig. 4(b). The peak centered at 100.7 eV corresponds to Si-C bond in SiC, while the peak at 101.8 eV can be assigned to SiO_xC_y [36], which is the intermediate product during the preparation of SiC nanoparticles. The same analysis results were obtained from the fine XPS spectra of Si 2p of SiC-B0, SiC-B4 and SiC-B8 (not shown).

Fig. 4(c) gives the fine XPS spectra of B 1s of SiC-B6 nanoparticles. Only one sharp peak appears at 189.8 eV, which can be assigned to the B-C bond in SiC [37, 38]. No peak is detected around 187.4 correspond to the B-Si bond and 193.1 eV correspond to the B-O bond [38], which indicates that B atoms have incorporated into SiC lattice and substituted Si sites. The same analysis results were obtained from the fine XPS spectra of B 1s of SiC-B4 and SiC-B8 (not shown).
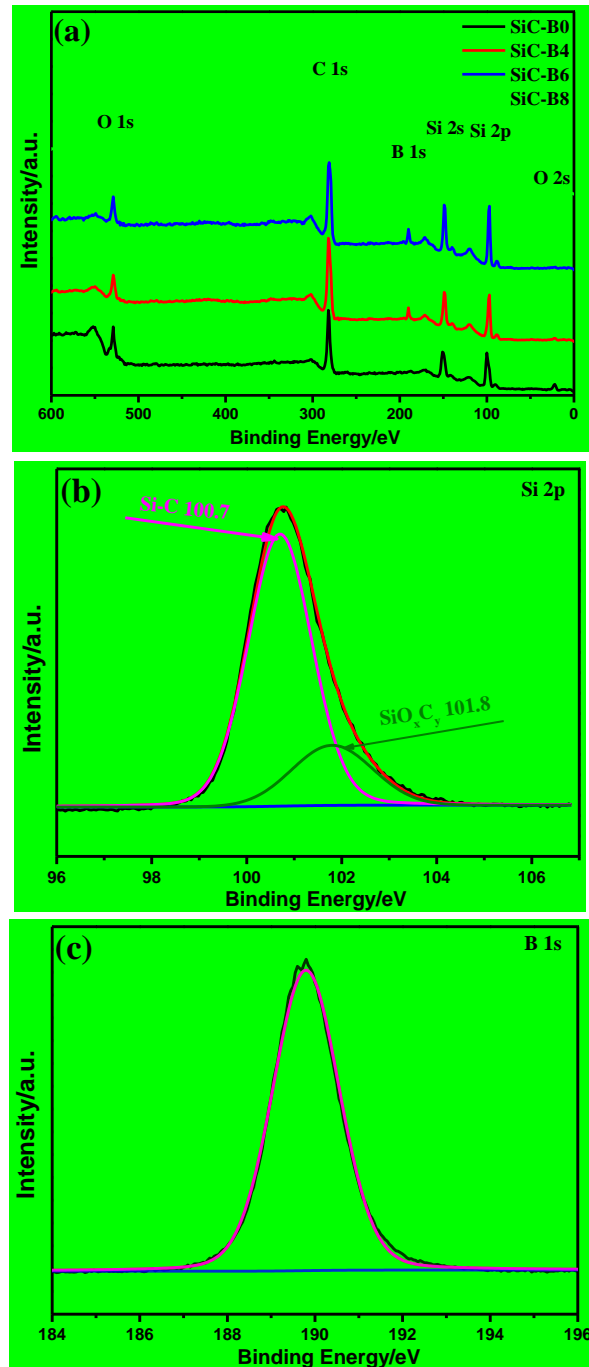

Fig. 4: XPS spectra of synthesized B doped SiC nanoparticles.

Fig. 5 gives the Raman spectra of the synthesized B doped SiC nanoparticles in the $600\sim1800$

cm^{-1} region. The Raman spectra shows the presence of sharp peaks at about 790 cm^{-1} and 966 cm^{-1} which correspond to transverse optical (TO) phonon mode and longitudinal optical (LO) phonon mode peaks of β-SiC, respectively [39]. The peak at 1590 cm^{-1} is related to the graphite structure of carbon residual in products, and the peak at 1355 cm^{-1} is similar to the TO peak of diamond, which is indicative of the presence of C–C sp3 bonds in β-SiC. Most probably the bonds are caused by carbon antisites in the SiC structure because of the lowest defect formation energy (1.1 eV) of C_{Si} in β-SiC. The peak intensities at 790 cm^{-1} and 966 cm^{-1} increase with the increasement of B dopant content. It indicates that B doping is beneficial to the crystallization of SiC, which is in agreement with the results of XRD [40]. Additionally, it can be find that the peak at 966 cm^{-1} (LO) shift to higher wavenumber obviously with the increased B dopant content. The LO peak will shift to higher wavenumber as the carrier concentration increases [41], so the LO peak shift of B doped SiC nanoparticles is due to the substitution for B atoms to Si atoms in SiC lattice to form B acceptor doping, resulting in the increase in the carrier concentration of holes. Because of the better crystallization of SiC with B doping, the peak intensity at 1355 cm^{-1} decreases with increasing B content, suggesting the decrease of the amount of C_{Si} defects in SiC crystallite. The peak intensity at 1590 cm^{-1} decreases with the increased B dopant content, which is due to the transformation of the sp2 carbon to the sp3 carbon due to the B doping [42, 43].
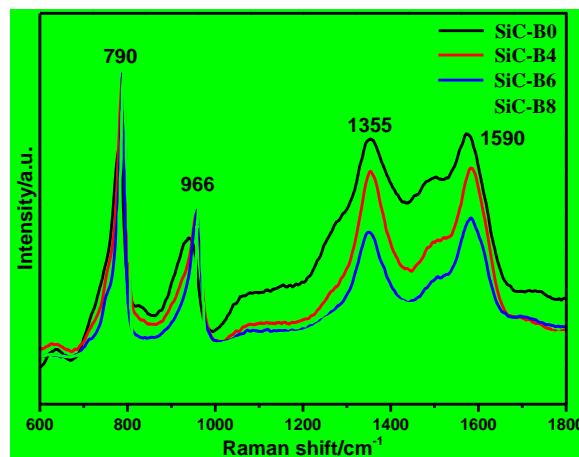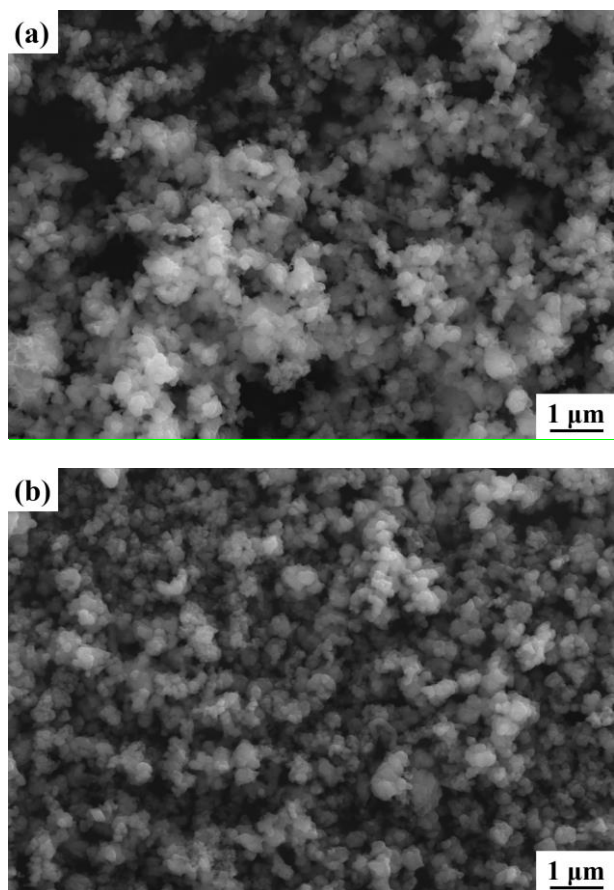

Fig. 5: Raman spectra of synthesized B doped SiC nanoparticles.

The typical microstructures of the obtained SiC-B nanoparticles observed by SEM are revealed in Fig. 6. From Fig. 6(a)-(c), the morphologies of SiC-B nanoparticles did not exhibit varied perceptibly with the increased B dopant content. SiC-B agglomerations consisting of large amount

nanoparticles were observed. Most of the nanoparticles were very smooth with equiaxed round shape. However, great grain growth was observed in the SiC-B8 sample (Fig. 6(d)). Large amount of micron grains with distinctly different shapes, such as plate like shape were observed demonstrating a higher crystallinity and grain growth. Such kind microstructure evolutions were in good agreement with the grain development of B doped SiC during the hot pressing processing and mechanical activation assisted self-propagating high temperature synthesis. It has been reported that the presence of B in SiC matrix could reduce the diffusion activation energy and enhance the mass transportation by several orders of magnitude which promoted the grain growth and crystallization of SiC grains [29, 44, 45]. Fig. 6(e) and Fig. 6(f) give the magnified images of SiC-B8 sample. Form Fig. 6(e), due to the increased tendency of the grains to be crystallized, many larger grains consist of multiple small grains can be seen in SiC-B8. The diameter of larger grains is often more than 1 μm, even close to 2 μm (Fig. 6(f)).

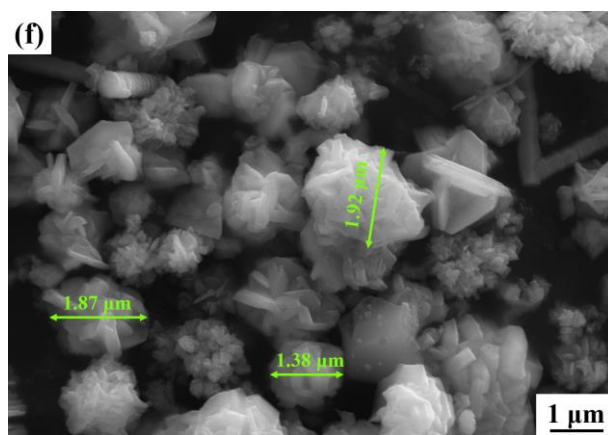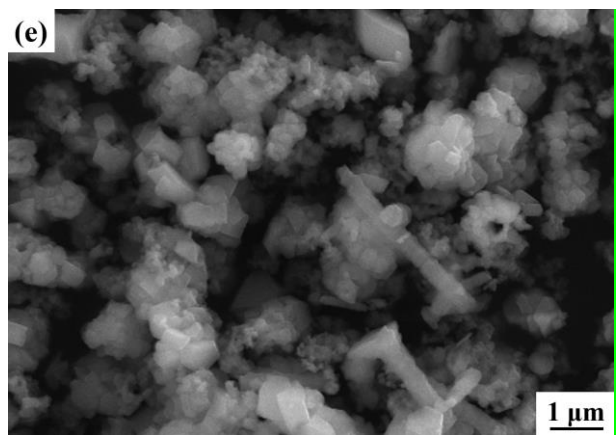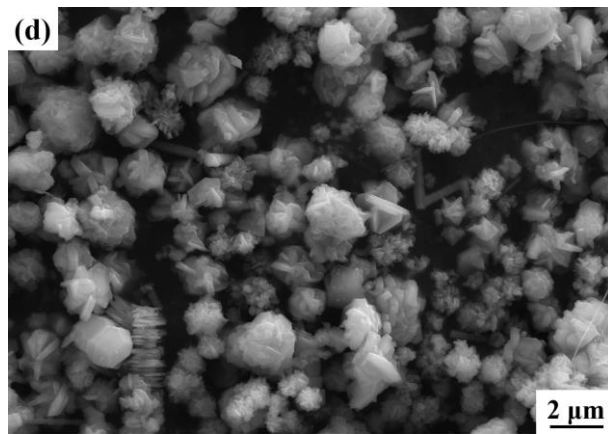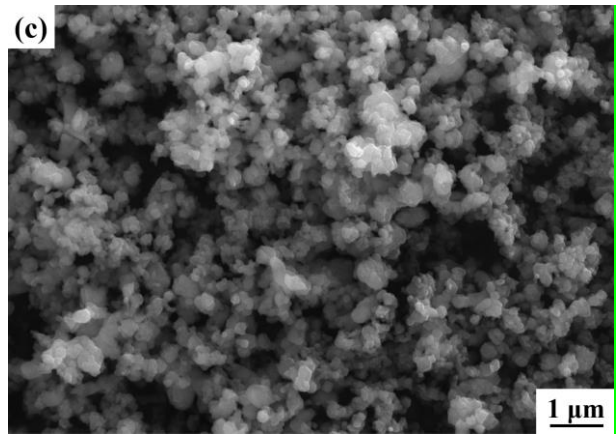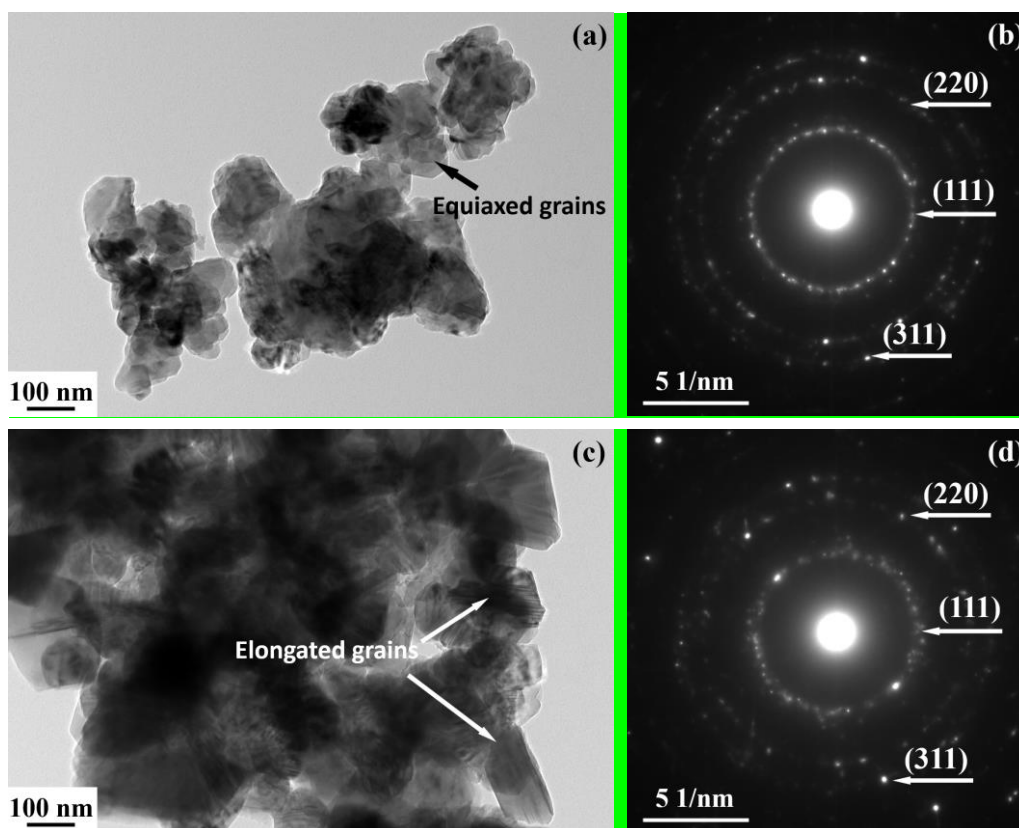Fig. 6: SEM micrographs of synthesized B doped SiC nanoparticles, (a): SiC-B0; (b) SiC-B4; (c) SiC-B6; (d) SiC-B8; (d) and (e): Magnified images of SiC-B8.

Indeed, the TEM observations and SAED analysis shown in Fig. 7 further confirmed such kind of microstructural evolutions. In the B free SiC nanoparticle (Fig. 7(a)), the grains are typically equiaxed shape with an average grain size of 116.33 ± 7.24 nm. However, in the SiC-B4 (not shown) and SiC-B6 nanoparticle (Fig. 7(c)), elongated grains with an average size of 172.80 ± 33.20 nm were observed which suggested better crystallization and grain growth. So, over doping B in the SiC phase would significantly promote grain growth. As shown in the Fig. 7(e), the grains of the SiC-B8 particles were grown into micron level which was in agreement with the SEM observation. Furthermore, SAED analysis also shows similar traces. Fig. 7(b) shows a representative diffraction ring of SiC nanoparticles. However, a clear increase of the diffraction spots was observed in the diffraction ring patterns of SiC-B6 (Fig. 7(d)) and Si-B8 (Fig. 7(f)) nanoparticles indicating the improved crystallization of the grains.
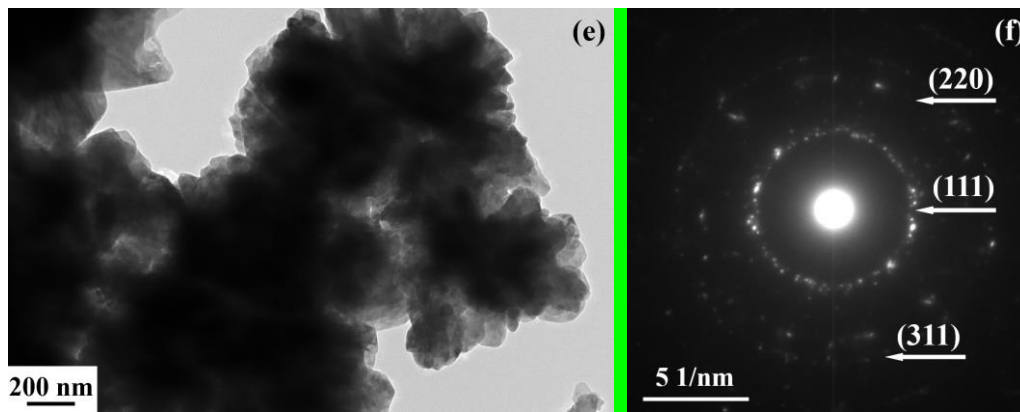
Fig. 7: TEM micrographs and SAED patterns of synthesized B doped SiC nanoparticles, (a) and (b) TEM image and SAED pattern obtained on SiC-B0 nanoparticles; (c) and (d) TEM image and SAED pattern obtained on SiC-B6 nanoparticles; (e) and (f) TEM image and SAED pattern obtained on SiC-B8 nanoparticles.

3.2 The surface property of SiC-B nanoparticles

The wettability and hydrophobic property of cubic SiC with different B dopant content are important factors for water based nanofluid. Water Contact Angle (WCA) are often used to qualify the properties. The measured WCA of SiC-B nanoparticles with varied B dopant content are shown in Fig. 8. In the B free SiC nanoparticles, the measured WAC was 115.50 °. However, in the B doped SiC nanoparticles, the measured WCA of all samples were reduced to almost close to 0 °, demonstrating that the particles with B dopant possessed good hydrophilicity. According to the wettability mechanisms, the wettability between the solids and liquid were strongly dependent on the surface energy of the solid particles. A solid with high surface energy could be easily wetted by liquid molecular which was due to the improved spreading parameter [46]. In our study, introducing minor B atoms to replace Si atoms, lattice distortions would take place in the SiC nanoparticles because a B atom only has three C atoms as neighbors [47]. On the nanoparticles surface and inside, the atoms near B atoms deviate from their original stable positions, enhancing the surface energy of SiC nanoparticles. Thus, the improved wettability and hydrophobic property of SiC-B nanoparticles might be due to the doping the boron into 3C-SiC phase surface which resulted in increase of the surface energy.
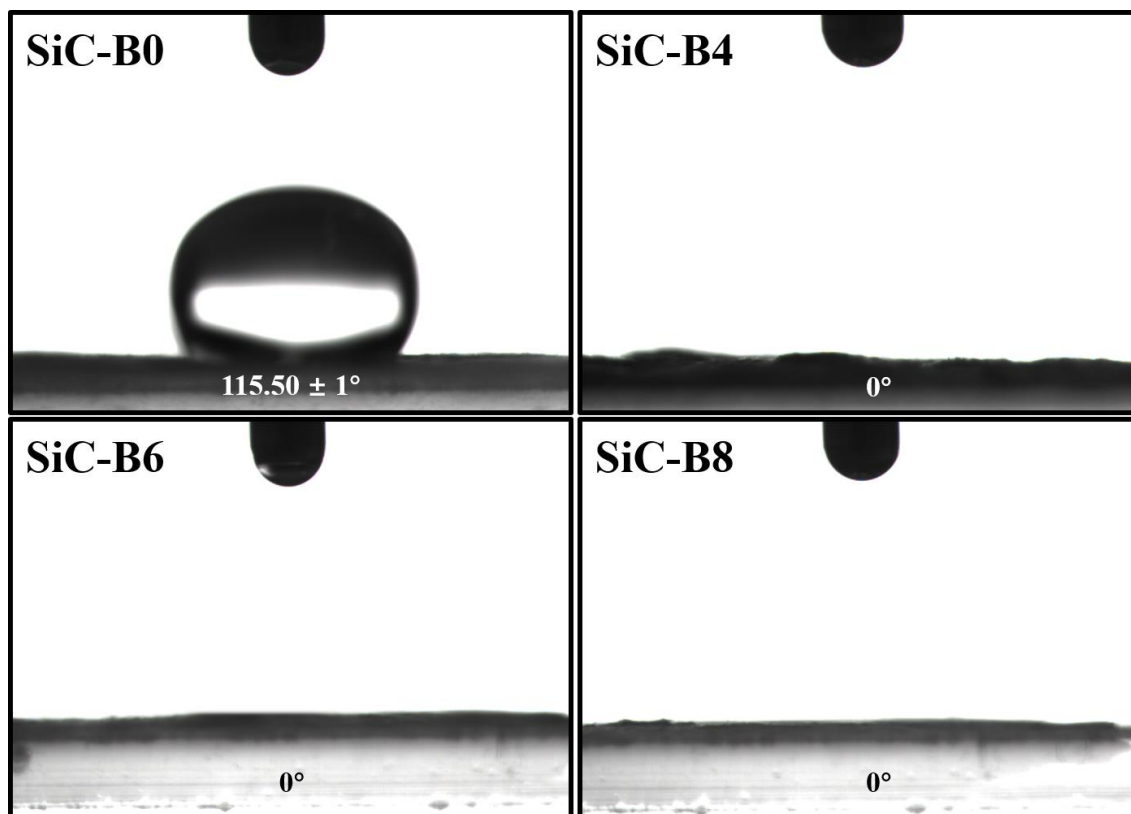
Fig. 8: Measured water contact angles of 3C-SiC-B nanoparticles.

3.3 Stability of SiC-B nanofluids

The stability of nanofluids is a critical factor that must be concerned because of the sedimentation and stratification of nanoparticles which would cause remarkable reduction of the TC of nanofluids and a Zeta potential analysis is commonly applied to evaluate the stability of the nanofluids. In general, a nanofluids with an absolute Zeta potential above 30 mV is considered to have moderate stability and those above 45 mV indicate good stability [22]. The pH value of fluid is a key parameter which affect the Zeta potential and dispersion stability of nanoparticles or colloidal. In order to investigate the stability region and identify the optimized pH values for stable dispersions, Zeta potential analyses of nanofluids containing 0.3 vol % SiC-B nanoparticles were measured in the pH region from 1 to 12 and is shown in Fig. 9(a). The Iso-Electric Points (IEP) for those B-doped SiC nanofluids were around pH 2.4-3.2 and the most stable dispersion was achieved at pH 11. At pH 11, absolute Zeta potential values of 35.5 mV and 23.5 mV were observed in the SiC-B0 nanofluid and SiC-B4 nanofluid, respectively, indicating a moderate stability while an absolute Zeta potential value of 53.5 mV was measured for SiC-B6 nanofluid revealing a superior stability. However, a

significant lower absolute Zeta potential (18.5 mV) was found in the SiC-B8 nanofluid. In the

previous study, it has been found the Zeta potential could be strongly affected by the particle size of

the dispersions. In the SiC-B8 nanofluid, particle size of the dispersions was over 1 μm, where

sedimentation and stratification became pronounced and significantly reduced the stability of the

nanofluids.

In addition, the concentration effect on the Zeta potential of the SiC-B nanofluids at pH 11 was

shown in the Fig. 9(b). In the 0.1-0.3 vol.% concentration range, the nanofluids with SiC-B6 was

found to have highest absolute Zeta potential values compared to the other B doping the SiC

nanofluids. The absolute Zeta potential value varied from 47 mV to 52 mV indicating a slight

enhancement of the stability with the increased SiC-B6 nanoparticle concentration. However, in the

other SiC-B nanofluids, the Zeta potential value did not show improvement within present

concentration range and the SiC-B8 nanofluids has the lowest Zeta potential value in the whole

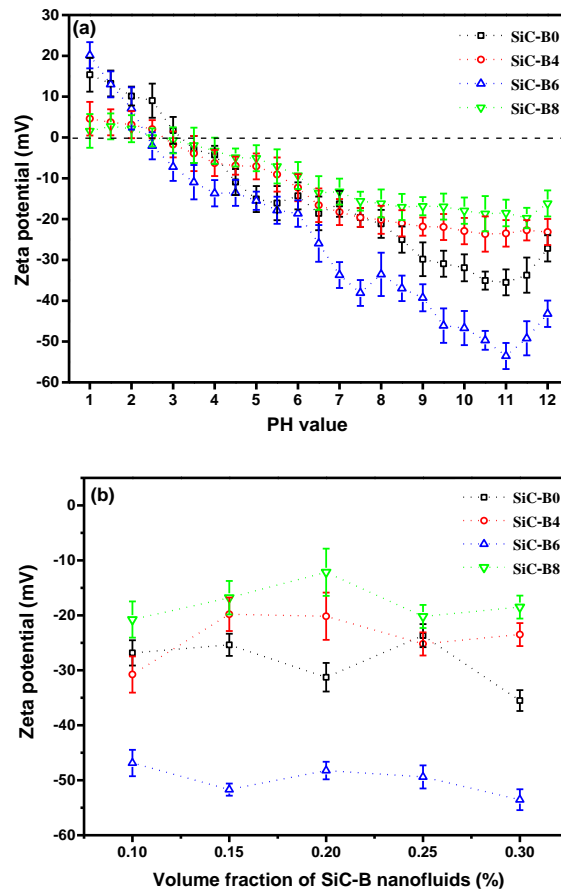range because of the presence of micron size particles.

Fig. 9: Zeta potential measurement of B-doped SiC nanofluids, (a) as a function of pH; (b) with

different volume fractions of SiC-B nanoparticle dispersions at pH 11.

According to the Beer–Lambert's law [48], the particles concentration is proportional to the absorbance of nanofluids. So, the reduction of particles concentration caused by the instability of nanofluids can be represented by the decrease in absorbance [49]. The relative concentration (C/C_0, the ratio of present concentration to initial concentration) of nanofluids was examined by using UV–vis to describe the stability of SiC-B nanofluids [50]. Fig. 10 illustrates the relative concentrations of SiC-B nanofluids versus time. In the first 3~6 days, the relative concentrations of SiC-B nanofluids decreased continuously, and then they tended to be stable. The SiC-B6 nanofluid exhibits excellent stability performance. In addition to the sedimentation of small amounts of unstable nanoparticles, it maintained a higher relative concentration of 94.72 % after 10 days. However, a very low relative concentration of 23.64 % was obtained from the SiC-B8 nanofluid after 10 days, indicating the poor stability, which is consistent with the analysis of Zeta potential. The sedimentation of many unstable larger particles reduced the relative concentration of SiC-B8 nanofluid. The relative concentrations of SiC-B0 and SiC-B4 nanofluids after 10 days are 69.53 % and 66.89 %, respectively, which are higher than SiC-B8 nanofluid and lower than SiC-B6 nanofluid. The final relative concentrations of SiC-B nanofluids are similar to their results of Zeta potential.
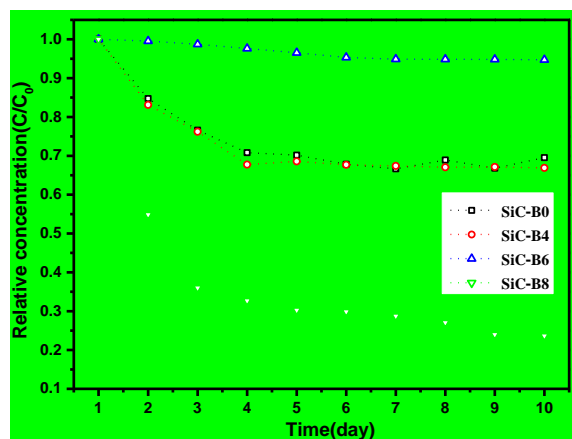

Fig. 10: Relative concentrations f SiC-B nanofluids versus time.

3.4 Thermal conductivity of water-based B-doped SiC nanofluids

The thermal conductivity of water based B-doped SiC nanofluids measured at temperature of 30 °C as a function of volume fractions is shown in Fig. 11(a). The TC values for B-doped SiC nanofluids are higher than that of the base fluids. Meanwhile, the TC of the B-doped SiC nanofluids were improved with the increased concentration of the dispersed nanoparticles in all cases. A remarkable

increase of the TC was observed in the SiC-B6 nanofluid with 0.3 vol.% concentration. Its TC

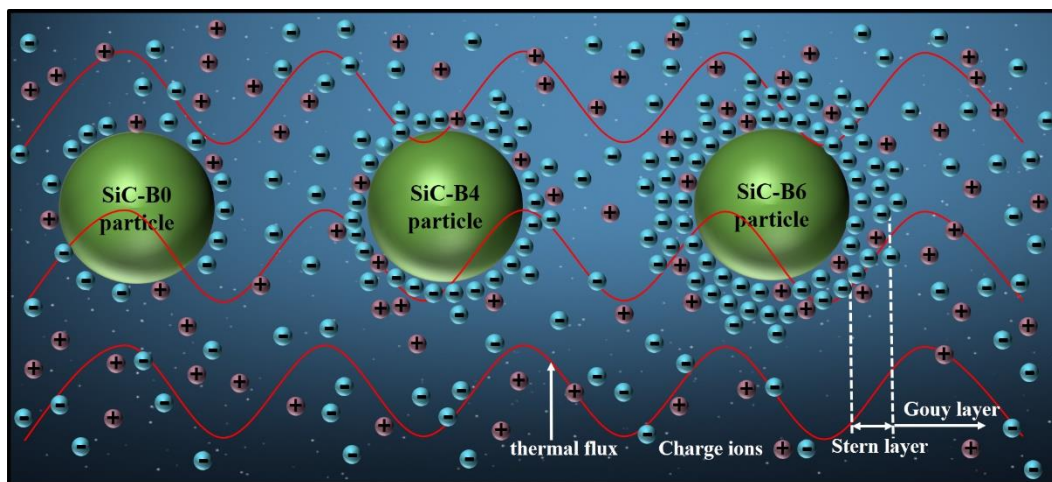increases to the highest 0.83 W/m·K with 39.3 % enhancement compare to the base fluids. Such

kind of TC improvement may be due to the better stability and enhanced thermal conductivity of

the SiC-B6 caused by the doping of B in the SiC lattice. However, in the SiC-B8 nanofluids, the TC

was significantly reduced due to the decreased stability which has been indicated by the Zeta

potential measurement. SiC-B8 has the largest crystal size and lowest Zeta potential may lead to

intense aggregation and sedimentation of SiC-B nanoparticle in the base fluid, leading to lower TC

value.

Fig. 11: Measured thermal conductivity of water based SiC-B nanofluids as a function of (a)

volume fractions of SiC-B nanoparticle dispersions; (b) temperatures (30-55 °C).

The higher Zeta potential of SiC-B6 nanofluids mean more charge ions are adsorbed on the

surface of nanoparticles in the same base fluid. Therefore,SiC-B6 nanoparticles possess the thickest

stern and gouy layer as shown in Fig. 12. When the nanofluid was working, the charge ions adsorbed

on the surface of nanoparticles transmit heat together with nanoparticles by thermal vibrations,

leading to enhanced thermal conductivity. Furthermore, by doping B in SiC, the TC of the SiC could

be improved. As discussed in the 3.1, the shrinkage of the SiC lattice parameter with the increased

B content suggested that the B element is preferably accommodated in the Si sites because of the

shorter atomic radius of boron. In the unit cell of the SiC, each C atom is connected to four

neighboring Si atoms and each Si atom is connected to four C atoms. Therefore, applying B as

dopant for the SiC, the B atoms will replace the Si atoms and will be connected with neighboring C

atoms. In this case, the difference in the valence between B^{3+} and Si^{4+} will create holes named

"bound holes" [29]. Those "bound holes" could accept electrons and favor thermal motion around the B atoms which can improve the TC of the SiC-B nanoparticles.

Fig. 12: Schematic diagram of thermal conductivity mechanism SiC-B0, SiC-B4 and SiC-B6 nanofluids

Furthermore, the TC of SiC-B nanofluids with 0.2 vol % nanoparticle concentration measured as a function of temperature is shown in Fig. 11(b). In a temperature range of 30～55 °C, the TC of SiC-B nanofluids was increased with the increasing temperature in all prepared nanofluids. A significant TC increase was observed in the prepared SiC-B6 nanofluids at 55 °C which was due to acute Brownian motion at higher temperature. Brownian motion of the nanoparticles became drastic with the increased temperature which could provide a much faster heat flow among particles leading to the enhancement of the TC [51]. Moreover, as shown in Table 2, compared with our previous work and aqueous or nonaqueous SiC nanofluids previously reported in the literature [17], SiC-B6 nanofluid with just 0.3 vol % in water can improve the thermal conductivity with the enhancement up to 39.3 % at 30 °C in this work, further verifying the promising application of SiC-B6 nanofluid as thermos-conductive fluids.

Table 2: Comparison of the thermal conductivity of SiC based nanofluids in the literature with this work.

Author	Nanofluid	Concentration	$100(k_{nf}-k_f)/k_f$

Xie et al. [11]	EG/SiC	4.0 vol %	22.90%
Chen et al. [17]	water/SiC	0.3 vol %	13.00%
Yu et al. [18]	EG/SiC	4.0 vol %	67.20%
Timofeeva et al. [19]	water/SiC	4.1 vol %	13.00%
Chen et al. [20]	saline water	0.4 vol %	5.20%
Li et al. [22]	Water/EG/SiC	1.0 vol %	33.84%
Li et al. [25]	EG/SiC	1.0 vol %	16.21%
Lee et al. [27]	water/SiC	3.0 vol %	7.20%
Ghanbarpour et al. [52]	water/SiC	1.0 vol %	29.00%
Singh et al.[53]	water/SiC	7.0 vol %	28.00%
This work	water/SiC	0.3 vol %	39.30%

4. Conclusions

B-doped SiC nanoparticles with varied B content were prepared by carbon thermal reduction reaction at 1500 °C in Ar. The doping of B into SiC phase leads to the shrinkage of crystal lattice of SiC and development of crystallization and grain growth of nanoparticles. From the Zeta potential measurement, a significant improvement of the stability was observed in SiC-B6 nanofluid at pH 11. However, poor stability was found in the over B doped SiC nanofluids (SiC-B8) because of the formation of micron size SiC-B particles which leaded to severe sedimentation and stratification. Furthermore, in the TC measurement of water based SiC-B nanofluids, the TC of the nanofluids containing only 0.3 vol.% SiC-B6 nanoparticles was remarkably improved up to 39.3 % at 30 °C compared to the base fluids and was further raised with the increased temperature. The improvement of TC of SiC-B6 nanofluids were ascribed to the more stable dispersion and more charge ions vibration on the surface of nanoparticles as well as the improvement of thermal conductivity of the SiC-B dispersions.

References

[1]   Pinto R V and Fiorelli F A S 2016 Review of the mechanisms responsible for heat transfer enhancement using nanofluids *Appl. Therm. Eng.* **108** 720-39

[2]   Haddad Z, Abid C, Oztop H F and Mataoui A 2014 A review on how the researchers prepare their nanofluids *Int J Therm Sci* **76** 168-89

[3]   Babita, Sharma S K and Gupta S M 2016 Preparation and evaluation of stable nanofluids for heat transfer application: A review *Exp. Therm Fluid Sci.* **79** 202-12

[4]   Taylor R, Coulombe S, Otanicar T, Phelan P, Gunawan A, Lv W, Rosengarten G, Prasher R and Tyagi H 2013 Small particles, big impacts: A review of the diverse applications of nanofluids *J. Appl. Phys.* **113**

[5]   Lee D, Park J-J, Lee M-K and Lee G-J 2017 Aging-resistant nanofluids containing covalent functionalized boron nitride nanosheets *Nanotechnology* **28** 405704

[6]   Ismail A M, Emara M M, El din Kassem T S and Moussa M A 2017 How assembly matters to catalysis and thermal conductivity mediated by CuO nanoparticles *Nanotechnology* **28** 075705

[7]   Karthikeyan A, Coulombe S and Kietzig A 2017 Wetting behavior of multi-walled carbon nanotube nanofluids *Nanotechnology* **28** 105706

[8]   Yoo D H, Hong K S and Yang H S 2007 Study of thermal conductivity of nanofluids for the application of heat transfer fluids *Thermochim. Acta* **455** 66-9

[9]   Izhevskyi V A, Genova L A, Bressiani J C and Bressiani A H A 2000 Review article: silicon carbide. Structure, properties and processing *Cerâmica* **46** 4-13

[10] Park C H, Cheong B H, Lee K H and Chang K J 1994 Structural and electronic properties of cubic, 2H, 4H, and 6H SiC *Phys Rev B Condens Matter* **49** 4485-93

[11] Xie H, Wang J, Xi T and Liu Y 2002 Thermal conductivity of suspensions containing nanosized SiC particles *Int. J. Thermophys.* **23** 571-80

[12] Roy S, Jacob C and Basu S 2004 Current transport properties of Pd/3C–SiC Schottky junctions with planar and vertical structures *Solid State Sciences* **6** 377-82

[13] Su J F, Niu Q, Tang C J, Zhang Y S and Fu Z X 2012 Growth of void-free 3C-SiC films by modified two-step carbonization methods *Solid State Sciences* **14** 545-9

[14] Eddy C R and Gaskill D K 2009 Silicon Carbide as a Platform for Power Electronics *Science* **324** 1398-400

[15] Wu R B, Zhou K, Yue C Y, Wei J and Pan Y 2015 Recent progress in synthesis, properties and potential applications of SiC nanomaterials *Prog. Mater Sci.* **72** 1-60

[16] Nikkam N, Haghighi E B, Saleemi M, Behi M, Khodabandeh R, Muhammed M, Palm B and Toprak M S 2014 Experimental study on preparation and base liquid effect on thermo-physical and heat transport characteristics of α-SiC nanofluids ☆ *International Communications in Heat & Mass Transfer* **55** 38-44

[17] Chen J H, Zhai F M, Liu M, Hou X M and Chou K C 2016 SiC nanowires with tunable hydrophobicity/hydrophilicity and their application as nanofluids *Langmuir* **32** 5909-16

[18] Yu W, Wang M Z, Xie H Q, Hu Y H and Chen L F 2016 Silicon carbide nanowires suspensions with high thermal transport properties *Appl. Therm. Eng.* **94** 350-4

[19] Timofeeva E V, Smith D S, Yu W, France D M, Singh D and Routbort J L 2010 Particle size and interfacial effects on thermo-physical and heat transfer characteristics of water-based α-SiC nanofluids *Nanotechnology* **21** 215703

[20] Chen W J, Zou C J, Li X K and Li L 2017 Experimental investigation of SiC nanofluids for solar distillation system: Stability, optical properties and thermal conductivity with saline water based fluid *Int. J. Heat Mass Transfer* **107** 264-70

[21] Li X K, Zou C J, Zhou L and Qi A H 2016 Experimental study on the thermo-physical properties of diathermic oil based SiC nanofluids for high temperature applications *Int. J. Heat Mass Transfer* **97** 631-7

[22] Li X K and Zou C J 2016 Thermo-physical properties of water and ethylene glycol mixture based SiC nanofluids: An experimental investigation *Int. J. Heat Mass Transfer* **101** 412-7

[23] Li X K, Zou C J and Qi A H 2016 Experimental study on the thermo-physical properties of car engine coolant (water/ethylene glycol mixture type) based SiC nanofluids *Int. Commun. Heat Mass* **77** 159-64

[24] Li X K, Zou C J, Wang T Y and Lei X Y 2015 Rheological behavior of ethylene glycol-based SiC nanofluids *Int. J. Heat Mass Transfer* **84** 925-30

[25] Li X K, Zou C J, Lei X Y and Li W L 2015 Stability and enhanced thermal conductivity of ethylene glycol-based SiC nanofluids *Int. J. Heat Mass Transfer* **89** 613-9

[26] Timofeeva E V, Yu W H, France D M, Singh D and Routbort J L 2011 Base fluid and temperature effects on the heat transfer characteristics of SiC in ethylene glycol/H_2O and H_2O nanofluids *J. Appl. Phys.* **109**

[27] Lee S W, Park S D, Kang S, Bang I C and Kim J H 2011 Investigation of viscosity and thermal conductivity of SiC nanofluids for heat transfer applications *Int. J. Heat Mass Transfer* **54** 433-8

[28] Yang T, Zhang L, Hou X, Chen J and Chou K C 2016 Bare and boron-doped cubic silicon carbide nanowires for electrochemical detection of nitrite sensitively *Sci Rep* **6** 24872

[29] Agathopoulos S 2012 Influence of synthesis process on the dielectric properties of B-doped SiC powders *Ceram. Int.* **38** 3309-15

[30] Kim K J, Lim K Y, Kim Y W and Kim H C 2013 Temperature Dependence of Electrical Resistivity (4–300K) in Aluminum- and Boron-Doped SiC Ceramics *J. Am. Ceram. Soc.* **96** 2525–30

[31] Gadzira M, Gnesin G, Mykhaylyk O and Andreyev O 1998 Synthesis and structural peculiarities of nonstoichiometric β-SiC *Diamond & Related Materials* **7** 1466-70

[32] Lutterotti L, Matthies S and Wenk H 1999 MAUD: a friendly Java program for material analysis using diffraction *CPD NEWSLETTER* **21** 14-5

[33] Mahbubul I M, Saidur R and Amalina M A 2012 Latest developments on the viscosity of nanofluids *Int. J. Heat Mass Transfer* **55** 874-85

[34] Log T and Gustafsson S E 1995 Transient plane source (TPS) technique for measuring thermal transport properties of building materials *Fire & Materials* **19** 43–9

[35] Su X L, Zhou W C, Xu J, Li Z M, Luo F and Zhu D M 2010 Improvement of permittivity of SiC with Al doping by combustion synthesis using Al_2O_3 *J. Alloys Compd.* **492** L16-L9

[36] Shimoda K, Park J S, Hinoki T and Kohyama A 2007 Influence of surface structure of SiC nano-

sized powder analyzed by X-ray photoelectron spectroscopy on basic powder characteristics *Appl. Surf. Sci.* **253** 9450-6

[37]   Dong L L, Wang Y Y, Tong X L, Jin G Q and Guo X Y 2014 Synthesis and characterization of boron-doped SiC for visible light driven hydrogen production *Acta Physico-Chimica Sinica* **30** 135-40

[38]   Oswald S and Wirth H 1999 Core-level shifts at B- and Al-doped 6H-SiC studied by XPS *Surf. Interface Anal.* **27** 136-41

[39]   Li Z M, Zhou W C, Su X L, Luo F, Huang Y X and Wang C 2011 Effect of boron doping on microwave dielectric properties of SiC powder synthesized by combustion synthesis *J. Alloys Compd.* **509** 973-6

[40]   Su X L, Zhou W C, Li Z M, Luo F, Du H L and Zhu D M 2009 Preparation and dielectric properties of B-doped SiC powders by combustion synthesis *Mater. Res. Bull.* **44** 880-3

[41]   Li Z, Zhou W, Lei T, Luo F, Huang Y and Cao Q 2009 Microwave dielectric properties of SiC(B) solid solution powder prepared by sol–gel *J. Alloys Compd.* **475** 506-9

[42]   Beeman D, Silverman J, Lynds R and Anderson M R 1984 Modeling studies of amorphous carbon *Phys. Rev. B* **30** 870-5

[43]   Richter A, Scheibe H J, Pompe W, Brzezinka K W and Mühling I 1986 About the structure and bonding of laser generated carbon films by raman and electron energy loss spectroscopy *J. Non-Cryst. Solids* **88** 131-44

[44]   Maître A, Put A V, Laval J P, Valette S and Trolliard G 2008 Role of boron on the Spark Plasma Sintering of an α-SiC powder *J. Eur. Ceram. Soc.* **28** 1881-90

[45]   Datta M S, Bandyopadhyay A K and Chaudhuri B 2002 Sintering of nano crystalline α silicon carbide by doping with boron carbide *Bull. Mater. Sci.* **25** 181-9

[46]   Gennes P G D 1985 Wetting: Static and Dynamics *Review of Modern Physics* **57** 827-63

[47]   Rurali R, Hernandez E, Godignon P, Rebollo J and Ordejon P 2004 First-principles studies of the diffusion of B impurities and vacancies in SiC *Phys. Rev. B* **69**

[48]   Aravind S S J, Baskar P, Baby T T, Sabareesh R K, Das S and Ramaprabhu S 2011 Investigation of Structural Stability, Dispersion, Viscosity, and Conductive Heat Transfer Properties of Functionalized Carbon Nanotube Based Nanofluids *The Journal of Physical Chemistry C* **115** 16737-44

[49]   Mehrali M, Sadeghinezhad E, Rosen M A, Akhiani A R, Tahan Latibari S, Mehrali M and Metselaar H S C 2016 Experimental investigation of thermophysical properties, entropy generation and convective heat transfer for a nitrogen-doped graphene nanofluid in a laminar flow regime *Adv. Powder Technol.* **27** 717-27

[50]   Sadeghinezhad E, Mehrali M, Akhiani A R, Tahan Latibari S, Dolatshahi-Pirouz A, Metselaar H S C and Mehrali M 2017 Experimental study on heat transfer augmentation of graphene based ferrofluids in presence of magnetic field *Appl. Therm. Eng.* **114** 415-27

[51]   Vajjha R S and Das D K 2012 A review and analysis on influence of temperature and concentration of nanofluids on thermophysical properties, heat transfer and pumping power *Int. J. Heat Mass Transfer* **55** 4063-78

[52]   Ghanbarpour M, Nikkam N, Khodabandeh R and Toprak M S 2015 Improvement of heat transfer characteristics of cylindrical heat pipe by using SiC nanofluids *Appl. Therm. Eng.* **90** 127-35

[53]   Singh D, Timofeeva E, Yu W, Routbort J, France D, Smith D and Lopez-Cepero J M 2009 An

investigation of silicon carbide-water nanofluid for heat transfer applications *J. Appl. Phys.* **105**